AN ABSTRACT OF THE DISSERTATION OF

Bret Bosma for the degree of Doctor of Philosophy in Electrical and Computer Engineering presented on July 16, 2013.

Title: On the Design, Modeling, and Testing of Ocean Wave Energy Converters.

Abstract approved: _____

Ted K.A. Brekken

Ocean wave energy converter technology continues to advance and new developers continue to emerge, leading to the need for a general design, modeling, and testing methodology. This work presents a development of the process of taking a wave energy converter from a concept to the prototype stage. A two body heaving point absorber representing a generic popular design was chosen and a general procedure is presented showing the process to model a wave energy converter in the frequency and time domains. A scaled prototype of an autonomous small scale wave energy converter was designed, built, and tested and provided data for model validation. The result is a guide that new developers can adapt to their particular design and wave conditions, which will provide a path toward a cost of energy estimate. This will serve the industry by providing sound methodology to accelerate the continued development of wave energy converters.

On the Design, Modeling, and Testing of Ocean Wave Energy Converters

by
Bret Bosma

A DISSERTATION

submitted to

Oregon State University

in partial fulfillment of
the requirements for the
degree of

Doctor of Philosophy

Presented July 16, 2013
Commencement June 2014

Doctor of Philosophy dissertation of Bret Bosma presented on July 16, 2013

APPROVED:

_____

Major Professor, representing Electrical and Computer Engineering

_____

Director of the School of Electrical Engineering and Computer Science

_____

Dean of the Graduate School

I understand that my dissertation will become part of the permanent collection of Oregon State University libraries. My signature below authorizes release of my dissertation to any reader upon request.

_____

Bret Bosma, Author

ACKNOWLEDGEMENTS

I would like to give special thanks to my advisor Dr. Ted Brekken for his guidance, support, and enthusiasm toward renewable energy research. Also, thanks goes to my committee members Dr. Annette von Jouanne, Dr. Ean Amon, Dr. Solomon Yim, and Dr. Joe Zaworski who all contributed significantly to my time here at Oregon State.

Thanks also goes to the whole Energy Systems Research group for being such a fun, strong, and focused team to work with. I would like to give special thanks to Doug Halamay and Chris Haller for their camaraderie in the lab. Thanks to Tim Lewis for a great collaboration on the AWEC project. Thanks to Stephen Zhang for all of the modeling help and wave energy discussions. Thanks to Kelley Ruehl for a great collaboration early on. In addition, I would like to thank the Northwest National Marine Renewable Energy Center, and specifically Belinda Batten and Meleah Ashford for their support during my time here. Thanks also to Manfred Dittrich for being patient with me and building an awesome prototype.

Finally, and most importantly, I want to thank my fiancé Emily, my Mom, and my Dad. Without your love and encouragement this would not have been possible. Thank you.

TABLE OF CONTENTS

TABLE OF CONTENTS (Continued)

Page

TABLE OF CONTENTS (Continued)

Page

TABLE OF CONTENTS (Continued)

Page

LIST OF FIGURES

Figure Page

LIST OF FIGURES (Continued)

Figure Page

On The Design, Modeling, and Testing of Wave Energy Converters

1 Introduction

The worlds growing energy demand coupled with climate change concerns have led to a resurgence of interest in renewable energy technologies [1]. It has become clear that we will need a host of solutions both renewable and non-renewable in order to keep up with world electricity demand. Solar and wind technologies have gradually matured with wind power becoming cost competitive in many energy markets. Ocean wave energy presents a vast, largely untapped, energy resource with the potential to add to the renewable energy mix.

Harnessing energy from ocean waves is not a new concept. The first patent of techniques for extracting energy from ocean waves dates back to 1799 [2]. The development of devices since has seen ups and downs including a resurgence in the 1970's with the research of Stephen Salter and the development of Salter's Duck [3]. Since then, there has been varying activity in the field with popularity and significant research increasing recently. Of note, Michael McCormick and Johannes Falnes have done pioneering research in the field.

The ocean provides the potential for an enormous untapped resource. In 2011 the Electric Power Research Institute (EPRI) did a study mapping and assessing the United States ocean wave energy resource [4]. They found that in total, electricity generation from waves could amount to more than 1170 TWh/year. That is near one third of the total annual consumption in the United States.

Ocean wave energy has many advantages. It is a renewable resource, generated ultimately from the sun. The sun causes uneven heating of the earth's surface which creates wind. Wind blown over the ocean surface creates waves. It is relatively predictable and consistent when compared to wind or solar. Although the resource can vary quite a bit seasonally, day to day the resource is relatively constant. It is also predictable in that sensors can be put out to sea and the resource at a location can be predicted as much as 48 hours in advance. Wave energy devices also typically have a low view shed. That is to say that typically most or all of the device is located under the water surface.

Ocean wave energy extraction can also pose many challenges. The ocean is a harsh environment and survivability is a key concern with extreme sea states and a caustic environment. There are also potential environmental effects including harm to wildlife and impact on sediment transport. Probably the biggest challenge to wave energy, however, is the high cost associated with the technology. The device cost itself is high and the deployment of the device is expensive. Operation and maintenance costs are high. Transporting the energy from the generation site to where it can be used is costly. For the wave energy industry to be successful these challenges will need to be addressed.

There are many ideas of how to extract the energy from the ocean waves with new concepts still being developed. Unlike the wind industry, where a horizontal two or three blade turbine has become the clear choice, there is a wide variety of wave energy technologies. These arise from the various ways that the energy can be absorbed from

the waves. Wave Energy Converters (WECs) can be classified in many ways including size, proximity to shore, and working principal [5].

In general there are three dominant types of devices, namely the oscillating water column, oscillating bodies, and overtopping type devices. Oscillating water columns can be split into near-shore fixed structures such as the Limpet, and off-shore floating structures such as the Oceanlinx. Oscillating bodies can be broken into floating types such as the PowerBuoy and submerged types such as the Oyster. Overtopping devices can be split into fixed structure types such as the TAPCHAN and floating structures such as the Wave Dragon.

One of the promising technologies which has attracted many developers is the heaving point absorber. A point absorber is defined as a device that has a horizontal extent much smaller than the incoming wave length. A relatively simple device, a heaving point absorber is an oscillating body which extracts the heave, or vertical motion from a wave. Point absorbers can be single-body or multi-body devices with hybrid type devices also possible.

Although the focus of this document is on the design, modeling, and testing of a heaving point absorber, many of the principals can be applied to other types of devices. For example, most systems will need hydrodynamic modeling as part of the design process. The concepts behind the frequency domain, time domain, and scaled wave tank testing will generally apply to other types of wave energy converters. Fig. 1.1 shows a block diagram of each major step in the process outlined in this document. The

tools used or developed are at the core of the diagrams and the necessary inputs and outputs are also shown.

The Oregon Wave Energy Trust has published an adaptation of the U.S. Department of Energy Guide that details Technology Readiness Levels (TRLs) for ocean wave energy devices [6]. These TRLs are from 1-9 and describe each phase in the process of commercialization of a wave energy converter. TRL 1 is basic technology research in which basic principles are observed and reported and TRL 9 is system operations at which the actual system is operated over its full range of expected conditions. Aspects of TRLs 1-5 are detailed in this document.

Chapter 2 describes frequency domain analysis and is the first step in the hydrodynamic modeling process. For this step everything is assumed to be linear, which has the benefit of speed and ease of implementation. Assuming linearity allows for rapid simulation times and is especially useful in shape optimization routines. Furthermore, frequency domain analysis can be the basis for a time domain analysis where nonlinearities can be introduced. This work falls into TRLs 1-2.

Chapter 3 outlines the time domain analysis which takes the frequency domain results and transfers them to the time domain. Among the advantages to this approach are the application of any input waveform that is desired and the introduction of nonlinearities to the system. This provides a higher level of detail of the operation of the system where performance results are closer to actual real world results. This work falls into TRLs 1-2.

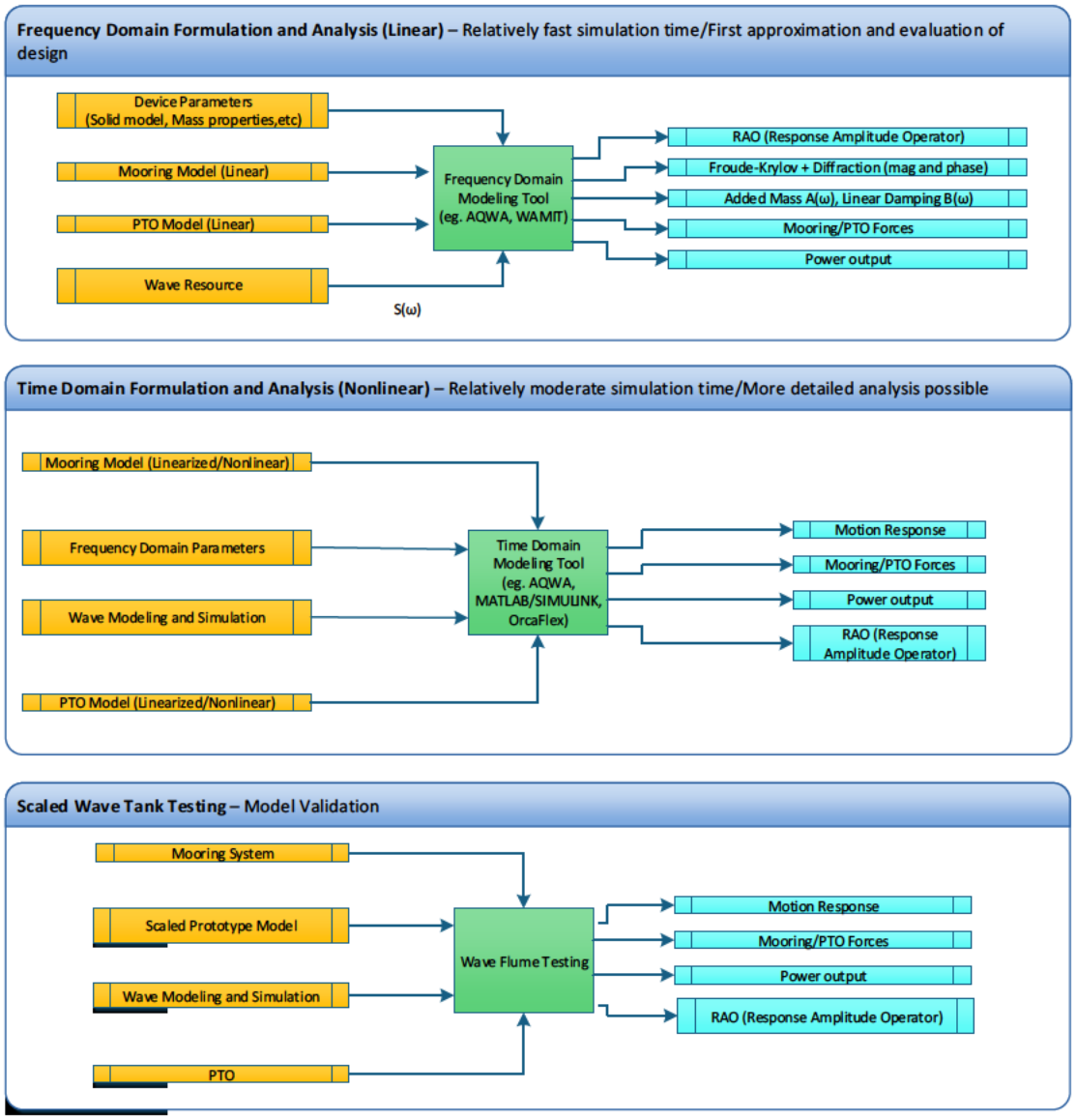

Fig. 1.1. WEC Design Flow Chart

Finally, Chapter 4 details Linear Test Bed (LTB) testing conducted at the Wallace Energy Systems and Renewables Facility (WESRF) and wave tank testing and model validation performed in the O.H. Hinsdale Wave Research Laboratory (HWRL). This is an extremely critical step in the design process because it provides confidence in the

time and frequency domain models and allows for calibration of these models. This work falls into TRLs 3-5.

This document is meant to serve as a guide, leading the reader from a concept through the prototype stage of development. Two modeling techniques which build in complexity are validated over certain operating conditions using scaled hardware wave tank testing. Although each device and details of implementation will undoubtedly be different, the general approach and underlying principals should apply.

2 Frequency Domain Analysis

2.1 Introduction

Wave Energy Converter (WEC) design is still in its infancy with significant research going into the design of new devices. Unlike the wind industry where a clear proven topology has been established, the wave energy industry is still looking for its first grid tied industrial scale wave generation site. As developers attempt to prove the merit of new designs a standard methodology is needed for the initial modeling of said devices.

Assuming that a rough physical WEC design has been chosen, frequency domain analysis is the first step in the validation of the merits of the design under operational sea conditions. In order to start a design, the detail of the end product does not need to be known, however the general shape and design philosophy is needed. The idea at this stage of the design process would be to create as simple a model as possible and start getting rough numbers for power output and performance characteristics. Several texts describing the theory behind ocean waves and structure interaction exist, which include [7],[8],[9]. Also, many papers on the subject exist, including [10],[11]. Development of a scaled wave energy converter is described in [12]. In addition, a numerical benchmark study of different wave energy converters is presented in [13].

Frequency domain analysis provides a good first step in the design process. Goals of frequency domain modeling include defining the parameters of the WEC, defining a mooring configuration and power take off system, and getting a first impression of how the device will perform. Because frequency domain analysis is intrinsically linear,

many real nonlinear effects which become prominent under high and extreme sea conditions are not taken into account and results should be viewed with this in mind [5]. More detailed analysis will no doubt follow, but frequency domain analysis provides an insightful look at a preliminary design and WEC performance for normal energy conversion operation. Basic shape optimization, identification of resonant frequencies of the device, structure loading due to wave pressures, general frequency response characteristics, and power output characteristics are to be gained by this analysis.

During the process of developing a WEC model, many results are relevant. In particular Response Amplitude Operators (RAOs), Froude Krylov forces, diffraction forces, added mass, and radiation damping forces in the frequency domain are useful. Hydrostatic results can also provide insight into the design. An iterative approach to changing shape design and characterizing the system can help improve the design, providing greater power output. This would be a first step in the process to estimate a cost of energy for the device.

For this project a generic two-body point absorber was used as an example of the design process. This is a popular design which several companies have pursued or are pursuing. Two general-purpose representative software products, ANSYS AQWA [14] and SolidWorks [15] were used in this modeling process, however several other modeling and hydrodynamics packages exist. Although these programs solve for motions (and forces) in six degrees of freedom, for convenience of exposition, focus in this presentation will be on the heave motion of a point absorber. Thus, only motion in

the z-direction will be analyzed. A high level block diagram of inputs and outputs of the representative model is shown Fig. 2.1.

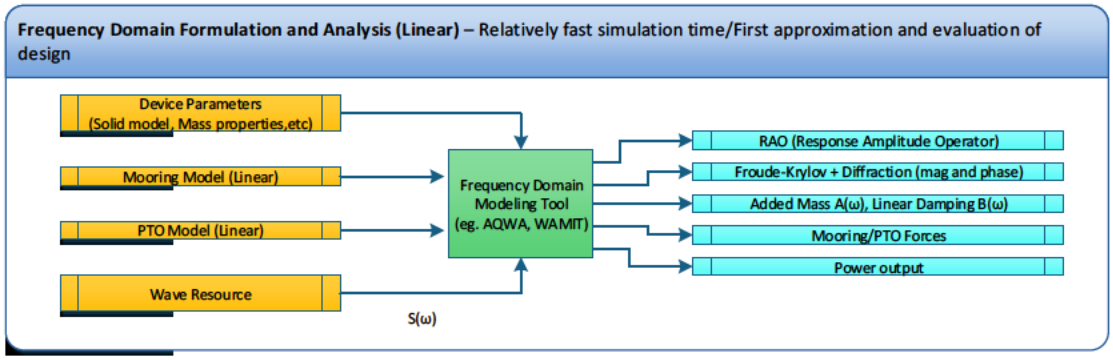

Fig. 2.1. High Level block diagram of inputs and outputs of frequency domain model.

This guide is targeted for researchers and wave energy converter companies that desire a methodology to follow in basic WEC design. It does not provide a novel design; rather it provides the background information and suggested techniques to expedite the process of designing a WEC.

2.1.1 Linear Wave Theory

A simple model of the waves is a good place to start defining the environment of a wave energy converter. Linear wave theory (also known as Airy wave theory) provides such a simple model, which assumes that the fluid flow is irrotational, incompressible, and inviscid, thus potential flow applies. It also assumes that the mean depth of water is uniform and that the wave amplitude is small. Airy waves can be modeled as the following

$$\eta(t) = A\cos(\omega t + kx) \tag{2.1}$$

where ω is the frequency in radians/sec and k is the wave number and $\eta(t)$ is the water surface elevation. The modeling at this stage utilizes these sinusoidal (also called harmonic) linear waves.

2.1.2 Forces on Structures

In order to ultimately define the potential power output from a wave energy device one must start with defining the forces acting on a structure. The governing equation of motion in the time domain is

$$M\ddot{z}(t) = F(t) \tag{2.2}$$

where M is the mass, z is the vertical displacement, and $F(t)$ are the total forces on the body. The types of wave forces on a body include viscous and non-viscous forces. The viscous forces include form drag and friction drag. Form drag is a function of the shape of the object. A body with a large apparent cross-section will have a larger drag than a body with a smaller cross-section, therefore presenting higher form drag. Friction drag is caused by the viscous drag present in the boundary layer around the body. The viscous forces including friction drag are usually relatively small in magnitude and neglected, or represented by a Morrison force term, and will not be discussed in this study.

Hydrodynamic forces exerted on the body, under the linear formulation, can be interpreted to include the Froude-Krylov force, diffraction force on a "fixed" body, and superposition of the radiation force due to the motion of the body. These forces arise from potential flow wave theory and linearization (which allows superposition of the linearized forces). The total (non-viscous) forces acting on a fixed floating body in

regular waves consist of the sum of the diffraction forces and the Froude-Krylov forces and are denoted as the excitation force as shown in equation (2.3). The Froude-Krylov force is a wave induced force on the "fixed" body, and its specification does not account for the effects of the presence of the body. It is the incident wave force resulting from the pressure on the virtual fixed body in the undisturbed waves. The diffraction force is due to scattering which is a combination of wave reflection and diffraction.

$$F_e(\omega) = F_{FK}(\omega) + F_d(\omega) \tag{2.3}$$

where F_e is the excitation force, F_{FK} is the Froude-Krylov force and F_d is the diffraction force. In this theory, an assumption is made that the dimensions of the body are sufficiently large in comparison to the wavelength of the incoming wave such that the incoming waves acting on the body are diffracted by the presentation of the body. The interpretation of the Froude-Krylov force is that the pressure field of the wave is not affected by the presence of the body is purely for convenience and is an artifact of linearization. The important physics that is enforced is that there is no flow through the (fixed) rigid body.

The radiation force due to structure motion can be decomposed into an added mass and a radiation damping term as shown in equation (2.4). This hydrodynamic force is induced by the structure's oscillation, which in turn generates waves. The "added mass" force component is in phase with body acceleration and the "radiation damping" term is in phase with body velocity. The added mass can be thought of as an added inertia on the body undergoing harmonic oscillation due to the presence of the surrounding fluid. The "radiation damping" is caused by the motion of the body in a fluid, generating

out-going waves carrying energy to infinity and in phase with the body velocity thus acting as a velocity proportional "damping force".

$$\mathrm{F_r}(\omega) = -\left(-\omega^2 \mathrm{M_a}(\omega) + \mathrm{j}\omega \mathrm{C}(\omega)\right)\mathrm{Z}(\omega) \tag{2.4}$$

where $M_a(\omega)$ is the added mass, $C(\omega)$ is the radiation damping, and $Z(\omega)$ is the heave motion and j is the imaginary unit.

The hydrostatic restoring or buoyancy force is exactly that, a force trying to return the structure to hydrostatic equilibrium. This force originates from the static pressure term because the wet surface of the body is exposed to varying hydrostatic pressures as a result of its oscillations. The hydrostatic stiffness is as follows

$$K = \rho g A' \tag{2.5}$$

where ρ is the density of the water, g is the acceleration of gravity, and A' is the cross-sectional area of the wetted surface. This leads to the definition of the hydrostatic force defined as

$$F_{hs}(\omega) = -KZ(\omega) \tag{2.6}$$

where $Z(\omega)$ is the frequency domain representation of the wave surface elevation at the device.

2.1.3 RAOs

Response Amplitude Operators (RAOs) are transfer functions which determine the effect a sea state will have on a structure in the water. This can be useful in determining the frequencies at which maximum amount of power can theoretically be

extracted. In order to calculate the RAO for a given structure a general equation of motion is defined.

$$-\omega^2 MZ(\omega) = F_e(\omega) + F_r(\omega) + F_{hs}(\omega) \tag{2.7}$$

where M is the mass of the structure, $F_r(\omega)$ is the radiation force, F_{hs} is the hydrostatic force, $F_e(\omega)$ is the excitation wave force (both incident and diffracting forces) and $Z(\omega)$ is the heave response. Fig. 2.2 shows the relationship between the terms in (2.7). This equation then leads to the RAO given as

$$RAO(\omega) = \frac{F_e(\omega)}{K - \omega^2\big(M + M_a(\omega)\big) + j\omega C(\omega)} \tag{2.8}$$

The RAO is a complex quantity and it is common to define the RAO as the magnitude of (2.8) when the phase difference between the incident wave and motion of the device is not of interest. However, the phase can be important in optimizing power output as a 180 degree phase shift between the float and spar velocity will maximize the generator speed.

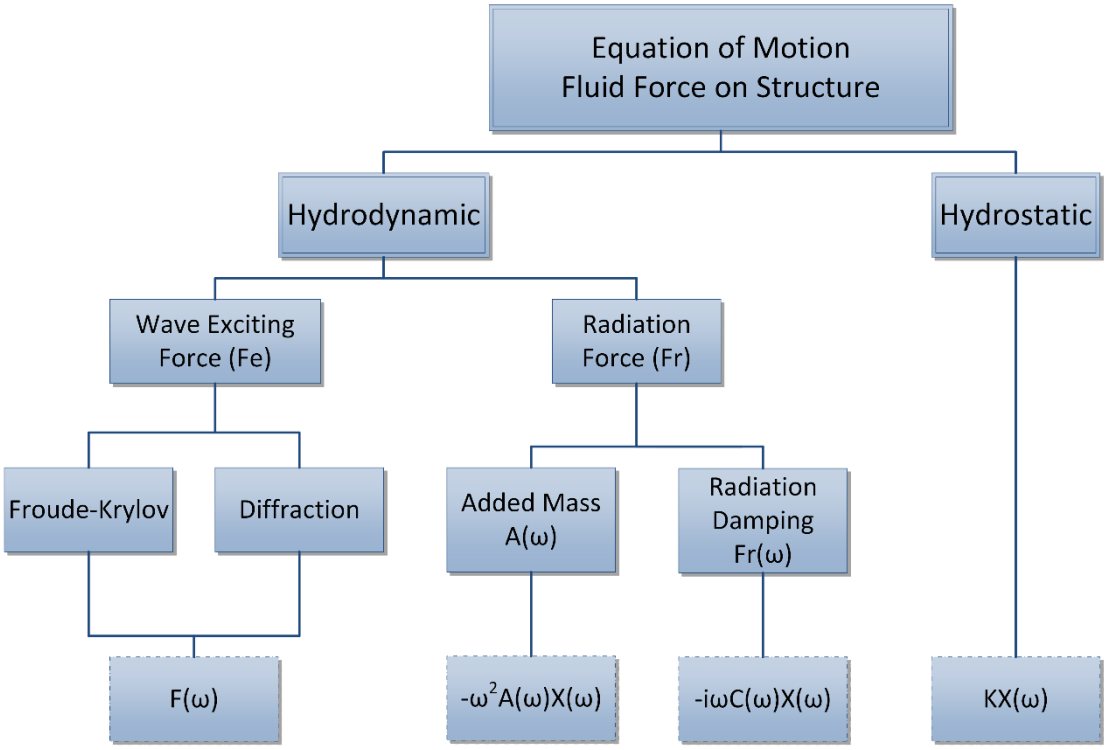

Fig. 2.2. Equation of motion terms of fluid forces on a structure.

2.1.4 Workflow

The workflow required to achieve frequency domain analysis will be useful for the designer in the design process. The first task is to create a computer model of the device to feed to the hydrodynamics package. Next, the hydrodynamics package would be applied. Although the approach outlined here is presented in the context of AQWA, the general approach can be applied to any hydrodynamics program with minor modifications. Post processing can also be achieved with many different tools. As an example of the process, MATLAB and Excel were used to post process the data provided by AQWA. The workflow decision tree for this design is shown in Fig. 2.3.

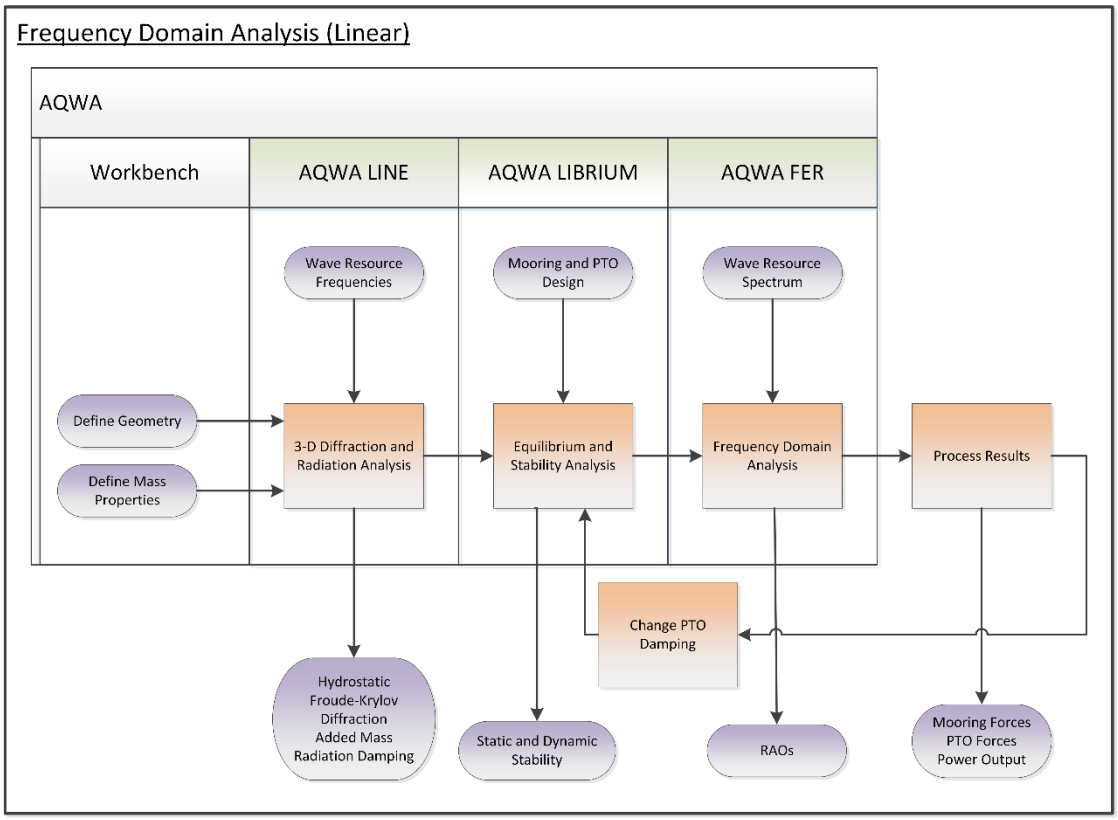

Fig. 2.3. Example workflow for frequency domain analysis.

2.2 Device Geometry

Given an idea for a wave energy converter, a computer model representation of the device needs to be created at this stage. There are different methods of defining device geometry. The method chosen is dictated by the hydrodynamics package selected. In this example a solid model approach is chosen using SolidWorks to define the geometry. For those using WAMIT, as another example, a surface model needs to be created. Ultimately, whichever program is used, a mesh of the device geometry will be defined. Fig. 2.4 shows an example of a WEC geometry. There are three bodies for this model, including a float, center spar, and damping plate. The center spar and damping plate

are locked together for the simulation. In a final design there would be a truss structure between the spar and damper but for initial simulation this is ignored.

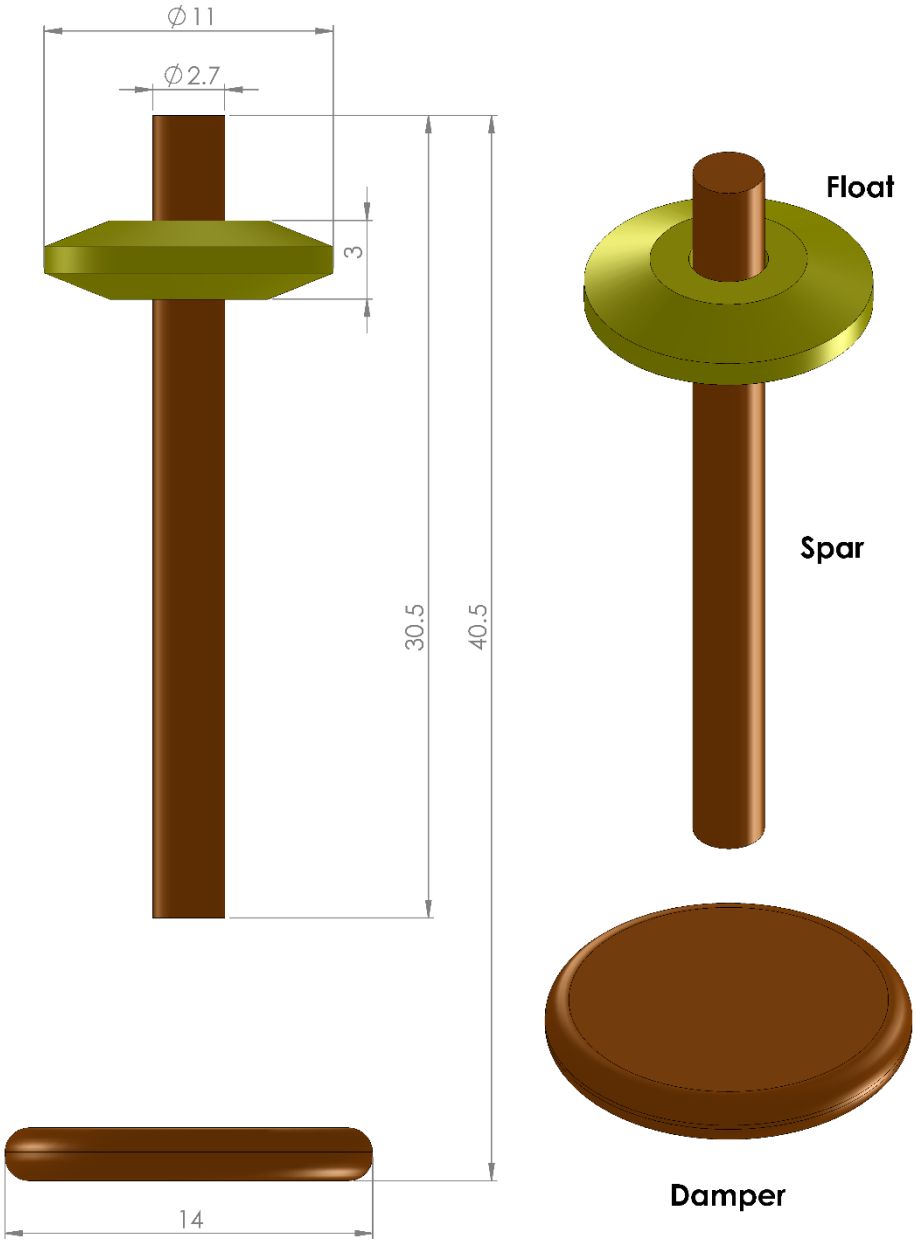

Fig. 2.4. Generic WEC example. A massless, stiff connection between the spar and damper is present, but not shown. All dimensions in meters.

2.2.1 Solid Model

Once a concept for a design is developed, the first step in analysis is creating a representation of the geometry of the device. This may take the form of a solid model, surface model, etc. In this example a solid model was used. There are several modeling packages available with which to develop a solid model. It is important to research the geometric formats required by the hydrodynamic tool that shall be used.

Beyond providing a convenient user interface for developing a model, packages such as SolidWorks can provide valuable information for model simulation such as the center of gravity of bodies, inertia values associated with bodies, and mass properties. As an alternative, many of the hydrodynamic software packages including ANSYS AQWA provide a simple modeling platform sufficient for creating basic shapes and devices.

Most WEC designs will be multi-bodied devices and in this case will be combined as an assembly of parts. In the generic point absorber example a separate body was created for the float, spar, and damper plate. The spar and damper are fixed together in the hydrodynamics package and the only relative motion is between the float and spar/damper. The reason for this has to do with the way that the hydrodynamic package deals with the interface between two bodies. If the proximity of two bodies is small enough, which is common in most WEC designs, the package requires time steps so small that it is not practical to run the simulation. Therefore, for this model, there will be three separate bodies, the float and damper plate will interact but there will be no interaction between the spar and the float.

Once the solid bodies have been modeled, characteristics such as inertia values and center of gravity can be gathered from the modeling program to be fed into the hydrodynamics program. When the geometry is imported into the solid modeling program the static water level needs to be defined and the body properties detailed. A point mass is defined for each body with the inertia values specified.

A big part of the modeling process includes generating a mesh with which the hydrodynamics program calculates the pressures and forces on each mesh element. This is where a tradeoff between model accuracy and simulation time and storage space needs to be made. Although a small mesh size would be preferred, a rougher mesh provides significantly shorter simulation times and smaller output files. Depending on the complexity of the bodies, and the patience for the simulation, a mesh size can be determined. The larger mesh size that is chosen, the faster results are obtained, however the smaller the mesh size, the more accurate the results will be. Take note that a single mesh size does not have to be used. A finer mesh can and was used near the interface between two bodies. This practice will lead to greater accuracy of results.

2.2.2 Mass Properties

Moments of inertia provide a measure of a bodies resistance to change in its state of rotation. For example, in a hydrodynamic package such as AQWA, mass and inertia values can be specified using a point mass approach. Inertia values can either be specified directly or via knowledge of the radius of gyration. This is calculated as the root mean square distance of the bodies parts from its center of gravity. SolidWorks calculates inertia values for the bodies that can then be transferred to AQWA. By

default the mass definition is program controlled so there is no need to input mass values. Alternatively, manually specifying the mass is an option.

The center of mass is the weighted average location of the mass of the body. For example, the center of mass is communicated as an XYZ coordinate into AQWA for each body. SolidWorks can be used to determine this center of mass using the mass properties dialog. This allows for simplified calculations by the hydrodynamics package by treating quantities as being referenced to the center of mass or treating a body as if its entire mass is concentrated at the center of mass.

Significant thought should be given to where the center of mass is located in the final design. For the device to be stable it needs to have a positive metacentric height. The metacenter is calculated as the ratio of the inertia resistance of the device divided by the volume of the device. At this stage however, device construction materials and all components are most likely not known. Therefore caution should be used to ensure that the center of mass is not in an unreasonable position.

2.3 Wave Resource Data

In conducting frequency domain analysis a range and number of frequencies is specified for a simulation. Hydrodynamic packages often by default have a program controlled setting for frequency range which can be modified to target a specific site if necessary. Water depth is also a critical parameter to be defined in the design process.

2.3.1 Range and Number of Frequencies

By default the range of frequencies may be program controlled by the hydrodynamics package. This will provide a range that will include most if not all conditions that the device might encounter. A total number of frequencies should also be chosen where more frequencies provide more detailed results.

If one wishes to target a specific site with a targeted range of frequencies this is possible. For example, the National Data Buoy Center (NDBC) [16] provides historical data for many locations around the world. For example, if a site near the NDBC Stonewall Banks buoy was chosen, historical data shows that a range of frequencies of 0.125 Hz to 0.3 Hz would capture the wave frequencies found at that site.

2.3.2 Wave Directions

Technically, if the device is symmetrical about the z-axis, there is no need to calculate multiple incident wave angles. In practice, however more accurate results will be obtained by choosing a number of incident wave angles. Increasing the number of angles has a relatively small impact on simulation time. A wave range, interval, and number of intermediate directions can be specified, all in degrees. For an asymmetrical device this can be a critical degree of freedom which further complicates the analysis results.

2.3.3 Water Depth

Water depth is a very important parameter in influencing power extraction of a WEC device. Power output in shallow water can be different from that found in deep water. From an analysis perspective, in general, a deep water assumption will make for

an easier process. However, if there is a desired location to target, or for specific scaled testing conditions it is important to use the depth in which the device will operate. For this example a deep water application was used with a depth of 1000 m.

2.4 Hydrodynamic Software Packages

There are several industry standard hydrodynamic codes available for analysis of WECs. These include WAMIT [17], ANSYS AQWA, and Orcaflex to name a few. There are also codes based on WAMIT such as WaveDyn and HydroD.

Both WAMIT and ANSYS AQWA solve the linear water wave boundary value problem. They use the Boundary Element Method (BEM), also known as the panel method and the integral method, to find diffraction and radiation velocity potentials. In general, BEM apply source or dipole functions on the surfaces of submerged bodies, and solve for their strength so that all boundary conditions are met [18]. Once the diffraction and radiation velocity potential fields have been solved, excitation forces, added mass and damping matrices, as well as wave field pressure, velocity, and surface elevation can be found. Both WAMIT and AQWA can also find hydrostatic forces and moments.

The primary difference between the two software packages is the data pre-processing, post processing, software interface, and supplementary calculations. WAMIT does not have a graphical user interface. Its inputs and outputs are text files that require pre-processing and post-processing by another program. AQWA does have a limited graphical interface that aids in part of the setup and analysis of a problem but

also uses text files for a significant portion of the modeling process. WAMIT users have high level of control over setup and access to a wide range of data outputs. AQWA has more post-processing computational tools including frequency domain analysis, time domain analysis, and stability calculations.

In the end, at this stage, the excitation force, added mass matrix, damping matrix, and hydrostatic coefficients need to be computed. Both WAMIT and AQWA compute these values with the same technique. It is left to the user to decide which software package is most comfortable, and whether additional data or analysis that is provided by a specific tool is needed.

The current codes intended for WECs have been adapted from the ship industry where ship dynamics have been studied. In general these vessels are much larger, single bodied structures. Although improving, sometimes the application of these codes to smaller, multiple bodies interacting, can lead to issues in convergence and accuracy. This can be partially attributed to the nonlinear effects which have a greater influence on the performance of the system at a smaller scale.

Hydrostatic results are also included in this stage. Center of gravity, volumetric displacement, center of buoyancy, and metacentric heights are some of the parameters available. These will help with keeping the proper stability of the device.

2.4.1 3-D Diffraction and Radiation Analysis

Once the solid model has been created and imported in the hydrodynamics package, the first step in analysis is a 3-D diffraction and radiation analysis. This will

determine wave force and structure response calculations as well as hydrostatic analysis. Outputs include the Froude-Krylov forces, diffraction forces, added mass, and damping forces in the frequency domain as shown in Fig. 2.5.

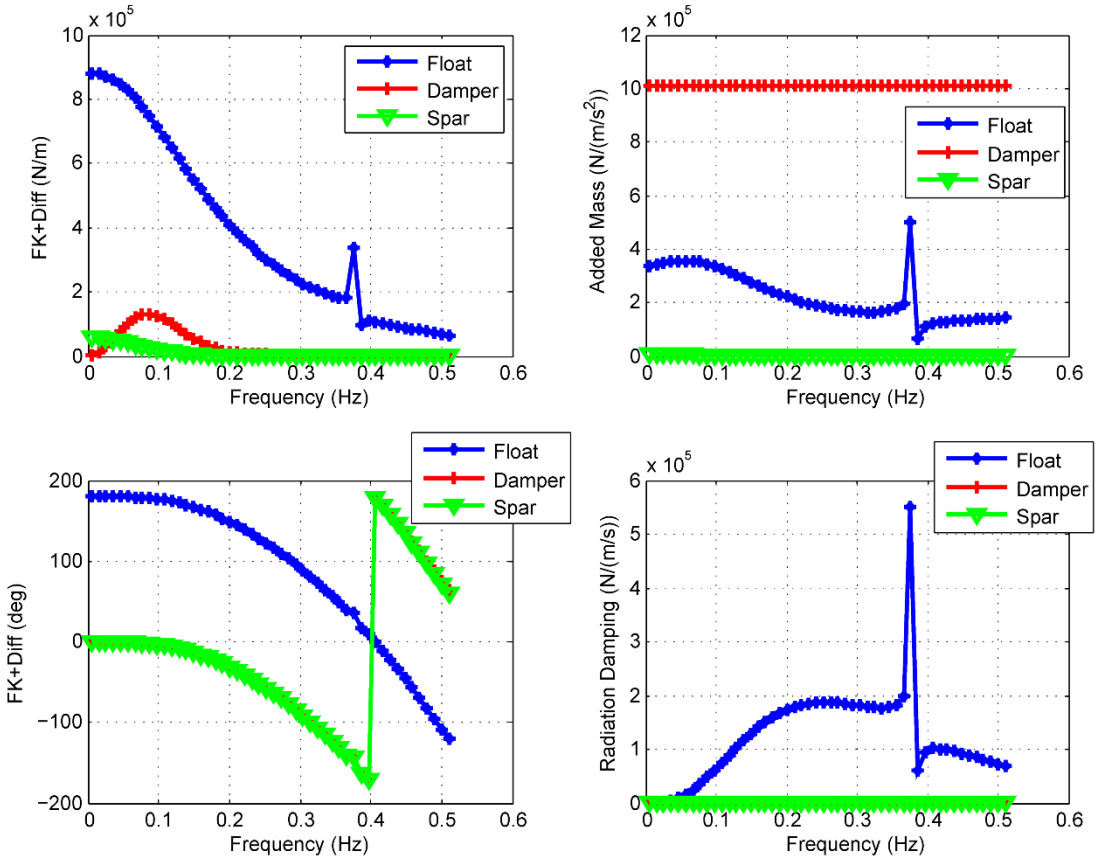

Fig. 2.5. Example 3-D Diffraction and Radiation Analysis results.

Note, at this stage, there is no mooring or PTO defined and the structures are not connected. This is acceptable for the device specific characteristics, namely the hydrostatics, Froude-Krylov, added mass, and radiation parameters. However if we would like to get information regarding the response amplitude operators, power generation, or mooring characteristics we will have to run further analysis.

2.4.2 Equilibrium and Stability Analysis

Equilibrium and stability is the next step in the process. Static equilibrium and stability of a system under the influence of the following steady forces: gravity, buoyancy, wave drift force, steady wind force, current, thrusters, and mooring are considered.

This is the stage where the mooring and power take off model gets introduced into the system. Equilibrium and stability analysis is necessary to move on to both frequency and time domain modeling.

2.4.3 Frequency Domain Analysis

Frequency domain response allows insight into the RAOs and relative velocity measurements which lead to power output calculations based on power take off implementation and mooring application. The hydrodynamic package calculates the significant response of amplitudes in irregular waves. It utilizes a linearized stiffness matrix and damping to obtain the transfer function and response spectrum. The major benefit of this type of analysis is the ability to make a systematic parameter study while getting power predictions for the device. At this stage, a mooring model and power take off need to be defined to simulate a more complete system. The following sections describe the models used.

2.4.4 Mooring Model (Linearized)

The mooring configuration used in this example is a three point system. The lines are assumed to be a conventional linear elastic cable. The lines are assumed to

have no mass and geometrically are represented as a straight line. The stiffness and the unstretched length are the two parameters that need to be specified.

Another option is a single point catenary mooring system. This can be modeled as a composite elastic catenary with weight. Mass per unit length and equivalent cross sectional area are properties that need to be defined for this type of mooring model.

There are many more possibilities for mooring a wave energy converter. The importance of mooring design and modeling should not be overlooked. Reference [19] shows many different mooring configurations with detailed analysis.

2.4.5 Power Take Off Model (Linearized)

One way to model a power take off (PTO) system is with an articulation allowing rotational motion. For this articulation a rotational damping term can be specified. Therefore, one must convert the rotational damping specified to an equivalent linear damping value to calculate the PTO force. Once that conversion has been made, calculating F_{pto}becomes

$$F_{pto}(\omega) = u_{rel}(\omega)B_l \tag{2.9}$$

where u_{rel} is the relative velocity between bodies and B_l is the linear damping value.

2.4.6 Response Amplitude Operators (RAOs)

The hydrodynamic package will provide a Response Amplitude Operator for each body. A sample output RAO magnitude and phase plot is shown in Fig. 2.6. As the plot shows the response drops off for waves with a period lower than around five seconds.

For example, if a monochromatic wave with an amplitude of 1 m and a frequency of 0.3 Hz is considered, the resulting heave motion of the float will have a magnitude of approximately 0.65 m and a phase shift of approximately 8 deg.

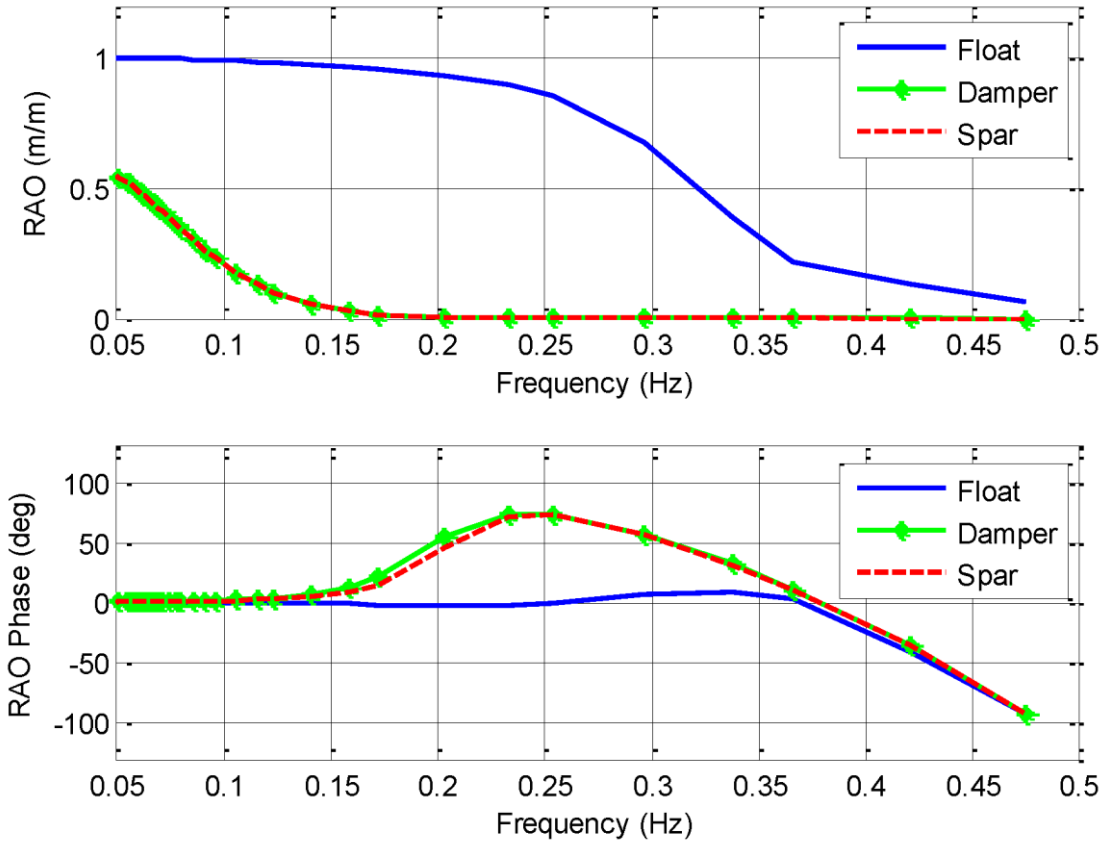

Fig. 2.6. RAO amplitude and phase for each body.

2.5 Output Power Comparisons

Once the PTO forces are known the next natural step is to calculate the power output of the device as a function of frequency for different damping values. The power for each frequency was computed using the following equation

$$P_{PTO}(\omega) = u_{rel}(\omega)\, F_{PTO}(\omega) \tag{2.10}$$

where u_{rel} is the relative velocity between the float and the damper and F_{PTO} is the force applied to the power take off.

Fig. 2.7 shows a sample of this output run for 50 damping values. An envelope was then developed to show the maximum power output for each frequency. Theoretically, what this shows is the amount of power possible if able to apply any damping value in the range of damping values that is tested. This shows possible resonance peaks around eight or nine second waves.

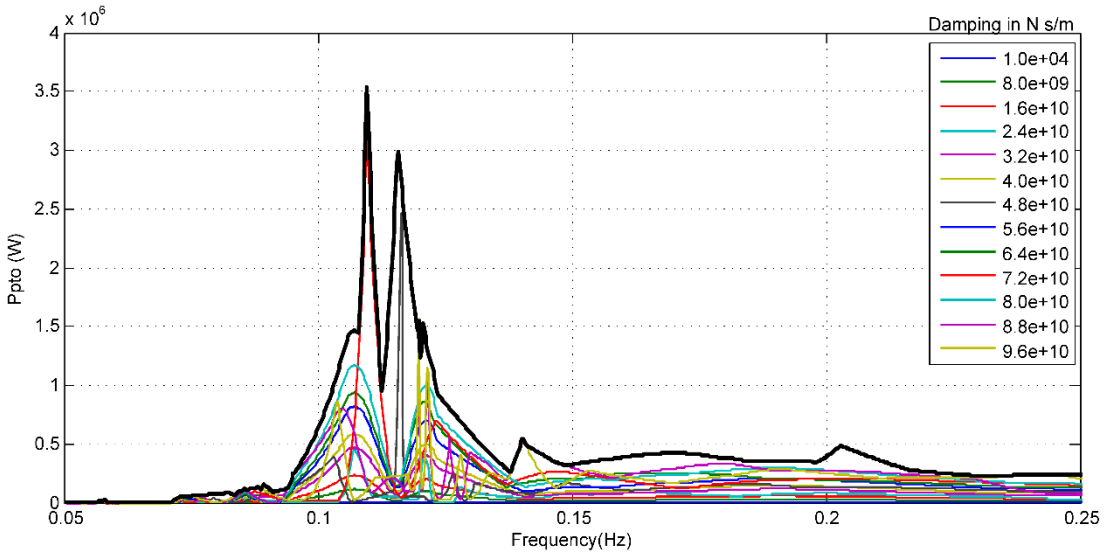

Fig. 2.7. Power vs. Frequency plot for multiple damping values, including envelope (thick black line) showing max power output for each frequency which could be achieved using active damping.

2.6 Conclusions

This chapter presents an outline of the necessary steps to perform frequency domain analysis on concept wave energy devices. The result is a guide showing a path from idea to potential power output values in the frequency domain. Targeted toward wave

energy converter device developers, it provides a clear methodology from concept to the first power predictions of a device.

3 Time Domain Analysis

3.1 Introduction

As the need for alternative energy sources increases, industries such as ocean wave energy, promising utility scale power generation from a renewable source, continues to grow. Wave Energy Converter (WEC) design is still in its infancy with significant research being applied to new designs. Thus far, no topology has provided a clear benefit over others in efficiency, cost of manufacture, maintenance requirements and production, thus new devices continue to be developed [5]. This is unlike the wind industry which has established a two or three blade horizontal axis wind turbine to be the most cost effective and efficient.

A good overview of the Ocean Wave Energy field is given in [9]. Many papers on the topic of time domain WEC modeling exist, including [20],[11],[10], but lack a clear design methodology. An attempt at benchmarking devices exists in [13]. The work presented in this document provides a clear time domain modeling approach of a heaving point absorber which can be adapted to other types of devices. A block diagram of the inputs and outputs of this stage is shown in Fig. 3.1.

3.1.1 Background

This document assumes that a rough physical WEC design has been chosen, and frequency domain analysis has already been performed as outlined in [21]. This can be achieved using any of the industry standard hydrodynamic software packages capable of doing frequency domain analysis. The next step in the validation of the merits of the

design is a time domain simulation derived from the frequency domain parameters of the WEC. A generic two body WEC is used in this document to provide an example of the necessary steps required to do the analysis. This analysis will give more realistic results for the response of the device than the frequency domain results were capable of providing.

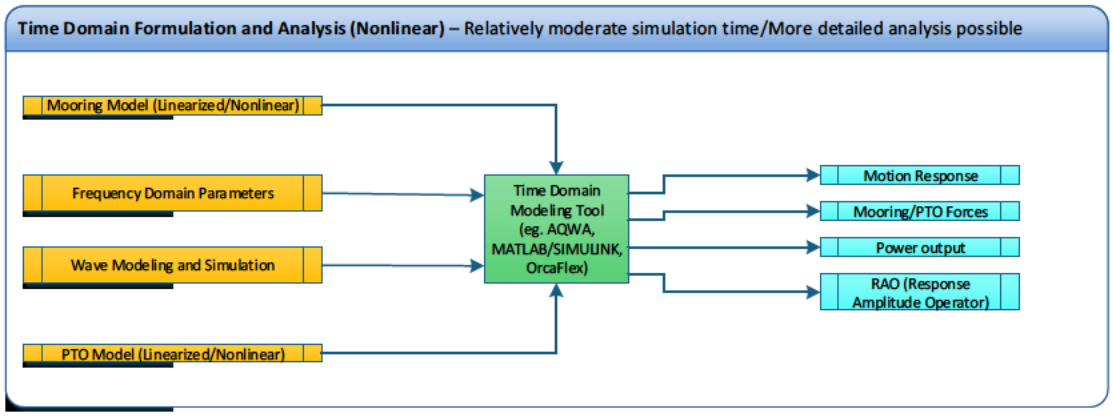

Fig. 3.1. Time domain formulation and analysis block diagram.

One benefit of time domain modeling is the introduction of nonlinearities to the model. This includes nonlinear mooring models as well as power take off (PTO) models. Such PTO nonlinearity could be realized by assuming that the linear damping has some limit of damping that can be applied. This manifests itself as saturation in the model.

Results of the time domain simulations include the motion response of the system (positions, velocities, and accelerations), the mooring and PTO forces, and a power output prediction. Throughout this document the assumption will be made that all calculations are in heave mode only.

3.1.2 Equations of Motion

The equations of motion can be obtained by summing the forces present on each body. The total forces which act on the heave motion of the structures can be broken down to many components. The excitation wave force, $F_e(t)$ is the summation of the Froude-Krylov force and the diffraction force and is the force imparted on the device by the incoming wave. The total radiation force, $F_r(t)$ is the force on the bodies due to structure motion and can be decomposed into an added mass term and a radiation damping term. The mooring force, $F_m(t)$ can be linearized or nonlinear, and can take on many different configurations. The hydrostatic force, $F_{hs}(t)$ is the force trying to restore the structure to hydrostatic equilibrium. The PTO force, F_{pto} is the force absorbed by the device to be converted to usable energy, and can be either linearized or nonlinear. The general equation is as follows

$$M\ddot{z}(t) = F_e(t) + F_r(t) + F_{hs}(t) + F_v(t) + F_m(t) + F_{PTO}(t) \tag{3.1}$$

as first introduced in [22] where M is the mass of the body.

The excitation force, $F_e(t)$ can be computed as a convolution of the water surface elevation and impulse response function from the frequency domain results obtained in previous simulations

$$F_e(t) = \int_{-\infty}^{\infty} \eta(\tau) F_t(t-\tau) d\tau \tag{3.2}$$

where $\eta(t)$ is the wave surface elevation at the WEC and

$$F_t(t) = \frac{1}{2\pi}\int_{-\infty}^{\infty} F(\omega)e^{j\omega t}d\omega \tag{3.3}$$

is the non-causal impulse response function of the heave mode, where $F(\omega)$ is the frequency domain summation of the Froude-Krylov force and diffraction forces. This presents a challenge because the excitation force at the current time is dependent on future input values. This is partially due to the wave impacting a part of the device prior to the wave impacting the point of analysis of the device as described in [23].

The radiation force, $F_r(t)$ can be computed as a convolution of the body velocity and the radiation impulse response function combined with the contributing force of the added mass at infinity of the body.

$$F_r(t) = -\int_{-\infty}^{t} k(t-\tau)\dot{z}(\tau)d\tau - m(\infty)\ddot{z}(t) \tag{3.4}$$

where

$$k(t) = \frac{1}{2\pi}\int_{-\infty}^{\infty} K(\omega)e^{j\omega t}d\omega \tag{3.5}$$

as shown in [23]. The integral in (3.5) is guaranteed convergence by subtracting off the added mass at infinity as shown in (3.6)

$$K(\omega) = R(\omega) + i\omega[m(\omega) - m(\infty)] \tag{3.6}$$

where $R(\omega)$ is the frequency domain radiation damping coefficients and $m(\omega)$ is the added mass of the body. Reformulation of (3.1) by moving the $m(\infty)\ddot{z}(t)$ term to the other side and defining F_r' as

$$F_r'(t) = -\int_{-\infty}^{t} k(t-\tau)\dot{z}(\tau)d\tau \tag{3.7}$$

becomes

$$\begin{aligned}\left(M + m(\infty)\right)\ddot{z}(t) \\ &= F_e(t) + F_r'(t) + F_{hs}(t) + F_v(t) + F_m(t) \\ &+ F_{PTO}(t)\end{aligned} \tag{3.8}$$

F_{hs} can be computed as the restoring force on the body attempting to bring it back to equilibrium as follows

$$F_{hs}(t) = \rho g A\, z(t) \tag{3.9}$$

where ρ is the fluid density, g, is the acceleration of gravity, and A is the water plane surface area.

F_v is the viscous friction forces on the body. Typically these are considered to be proportional to the velocity of the body and are determined experimentally.

F_m is the mooring force and can take many forms. Mooring configurations can be very complicated and highly nonlinear. For this paper a simple catenary mooring is considered in the form of a spring

$$F_m(t) = -K_m z(t) \tag{3.10}$$

where K_m is the spring constant of the mooring.

3.2 Model to be Analyzed

For this research a generic two body point absorber was chosen as shown in Fig. 3.2. It is assumed that a frequency domain analysis has already been performed as outlined in [21]. Therefore the geometry has already been chosen and results from the frequency domain analysis have already been obtained.

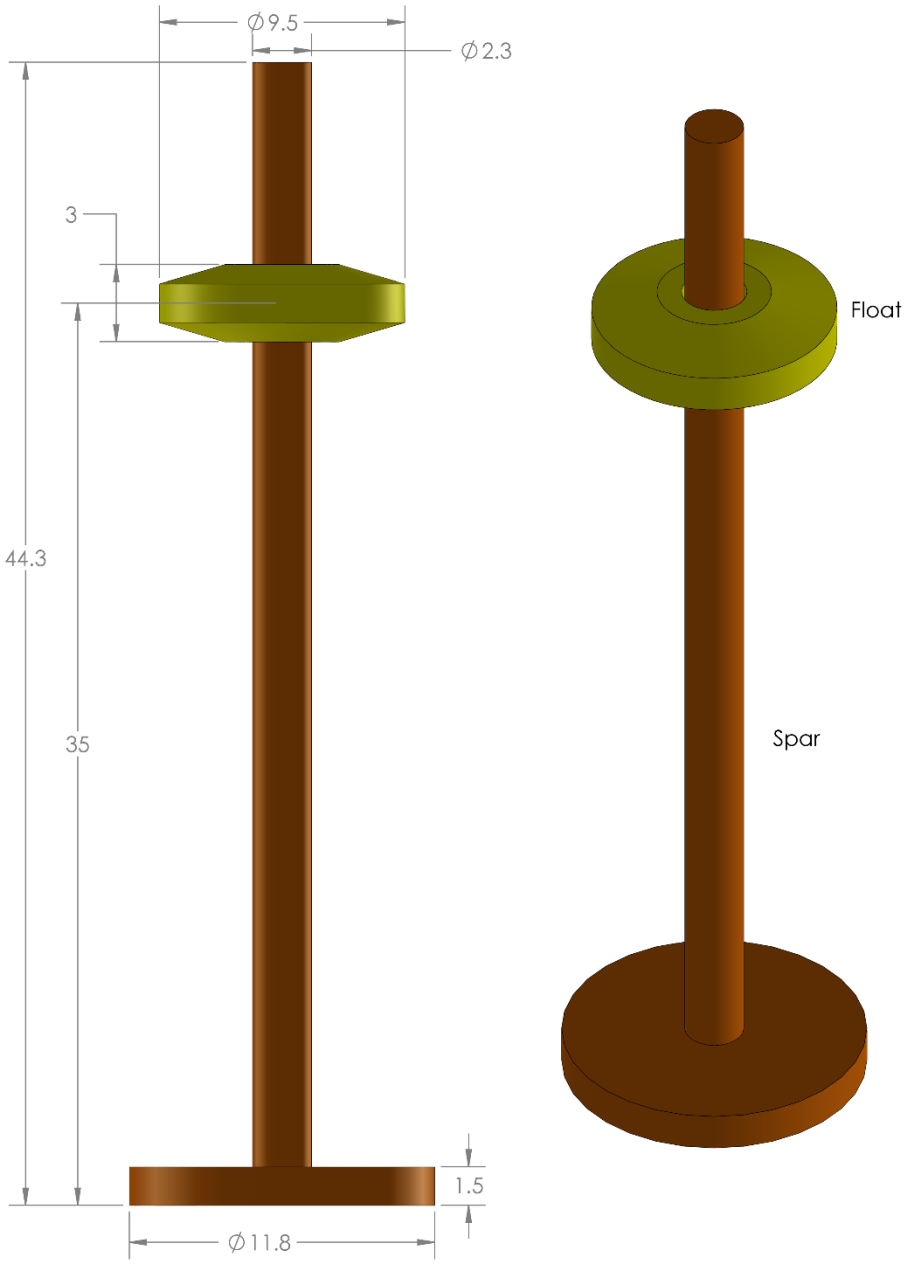

Fig. 3.2. Generic WEC example. All Dimensions in meters.

The pertinent frequency domain parameters needed for the time domain simulation include the following.

- The Froude Krylov plus diffraction frequency domain coefficients describing the resulting forces on a body imparted by an incoming wave.
- The radiation damping coefficients describing the motion of the body in a fluid, generating outgoing waves in phase with the body velocity thus acting as a velocity proportional damping force.
- The added mass coefficients defined as the added inertia on a body undergoing harmonic oscillation due to the presence of the surrounding fluid.

3.3 Input Waves

It is possible and insightful to simulate both regular (monochromatic) and irregular (spectrum) waves in the time domain simulation. Regular waves give a controlled input that is repeatable and the response for the given input easily identified. Irregular waves provide a more realistic representation of what the WEC would face in real seas.

3.3.1 Regular Waves

For regular wave input, a sinusoidal (also called harmonic) linear wave can be defined as shown in the following linear wave input.

$$\eta(t) = Acos(\omega t) \tag{3.11}$$

where ω is the frequency in radians/sec, and $\eta(t)$ is the water surface elevation at the WEC in meters.

3.3.2 Irregular Waves

For irregular wave input, typical wave spectra include Jonswap, Pierson-Moskowitz, Bretschneider, and Gaussian, distribution [24]. These wave inputs are all uni-directional. A typical treatment of the spectrum is as follows. The spectrum is split into N sections of equal area. N wavelets with frequency at the centroid of the section are defined with N having a maximum of 200. The wavelets are then added together with random phase angles taking on the following form

$$\eta(t) = \sum_{i=1}^{N} a_i \cos(\omega_i t + \phi_i) \tag{3.12}$$

For an example of a Pierson-Moskowitz input the following need to be specified. The wave direction, the range of frequencies to be included, the significant wave height, zero crossing period, and a seed used to define the random seed for a wave spectrum must be included. For simulation purposes the resulting time series can be input into the simulation.

3.4 Time Domain Differential Equation Solver Approach

One method for modeling a two body wave energy converter is by using a solver to solve the equations of motion and then calculate outputs from that simulation. These equations of motion describe the motion of the individual bodies due to many forces as shown in the introduction to this paper. The dominant forces which are present in an actual wave energy converter model and will be outlined here. We are considering a device with two bodies and therefore will have two equations of motion, one for each

body. Subscript 1 will refer to the float and subscript 2 will refer to the spar as shown in Fig. 3.3.

Fig. 3.3. MATLAB/Simulink implementation of equations of motion for two body WEC.

Additional forces include a viscous damping force, a power take off force, and mooring forces. With the addition of these forces, the equations of motion in the heave direction for each body take the form

$$F_{e1}(t) - F_{r11}'(t) - F_{r21}'(t) - F_{hs1}(t) - F_{pto}(t) - F_{v1}(t) = \left(M_1 + m_1(\infty)\right)\ddot{z}(t) \tag{3.13}$$

$$F_{e2}(t) - F_{r22}'(t) - F_{r12}'(t) - F_{hs2}(t) + F_{pto}(t) - F_{v2}(t) - F_m(t) = \left(M_2 + m_2(\infty)\right)\ddot{z}(t) \tag{3.14}$$

where $F_{e1}(t)$ is the force imparted by the incoming wave on body 1, $F_{r11}(t)$ is the radiation force imparted on body 1 as a result of the waves created by body 1, $F_{r21}(t)$ is the radiation force imparted on body 1 as a result of the wave created by body 2, $F_{hs1}(t)$ is the hydrostatic stiffness force on body 1, F_{pto}(t) is the electromechanical force on body 1 from the generator acting as the power take off, and $F_{v1}(t)$ is the force from viscous friction on the body. The second equation takes the same form as the first with the exception of the sign on the PTO force and the addition of the mooring force attached to body 2.

These equations were then input into MATLAB/Simulink as shown in Fig. 3.3. Note that there are two similar structures of computation, one for each body. The excitation forces, radiation forces, and hydrostatic forces are calculated in subsystems which will be detailed below.

The excitation force calculation F_e, as shown in equation (3.2), is shown in Fig. 3.4. First the impulse response function is calculated by solving the integral as shown in equation (3.3) using the parameters obtained by a software package such as ANSYS AQWA[14] or WAMIT[17]. The resulting non-causal impulse response function is

then split into its causal part and non-causal part and convoluted with the wave surface elevation η as shown in equation (3.2). In Simulink, the convolution is implemented using the finite impulse response filter block with the impulse response function parts fed as coefficients.

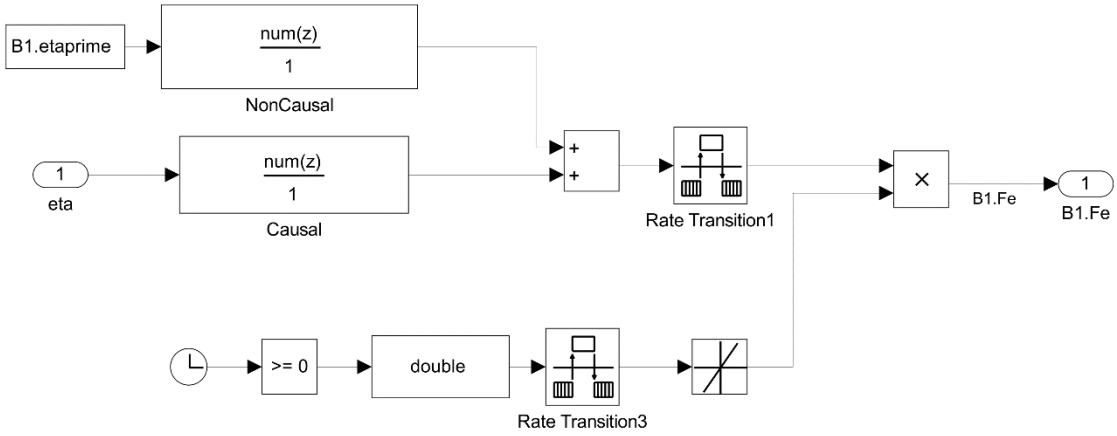

Fig. 3.4. Excitation Force convolution.

Notice that the input waveform was broken into a causal and a non-causal part which are convoluted separately and the results added together. Also notice that a rate limiter was used to ease the excitation force into the simulation. This is necessary because of the non-causal nature of the excitation force. The radiation force has a similar structure, however as the impulse response function is causal in nature, it requires just one convolution.

The most common and straight forward initial model for the power take off is as a linear damping. Its implementation in the model becomes a constant damping gain that is multiplied by the relative velocities between the two bodies which provides the power take off force calculation. Although this is convenient and a relatively accurate and

effective control scheme for some regions of operation, introduction of nonlinear damping parameters can both provide a more realistic model of the system and could potentially improve the power output from the device.

3.5 Simulation Results

Simulation of a two-body WEC was performed with both regular and irregular wave inputs. Two different power take off damping schemes were employed for regular waves. The first, linear damping produced a sinusoidal output in displacement, force, and power, as expected and shown in Fig. 3.5. The second, saturated linear damping, implemented limits on the damping applied and effectively clipped the force applied to the power take off and thus the power produced as shown in Fig. 3.6. Due to this non-linearity, this analysis cannot be done in the frequency domain.

The same set of damping conditions were then applied to an input of irregular sea data as shown in Fig. 3.7 for linear damping and Fig. 3.8 for saturated linear damping where the nonlinear clipping of the signal is clearly shown.

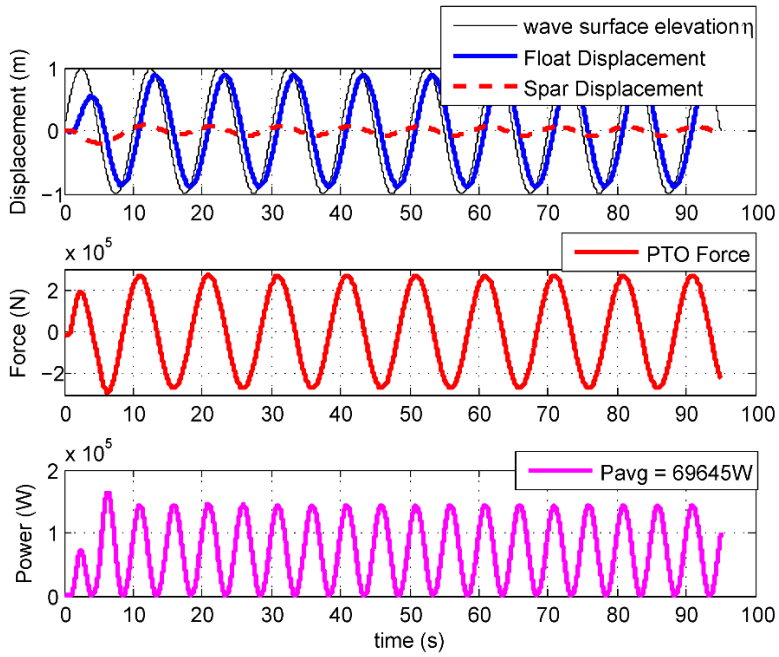

Fig. 3.5. Linear damping regular wave input.

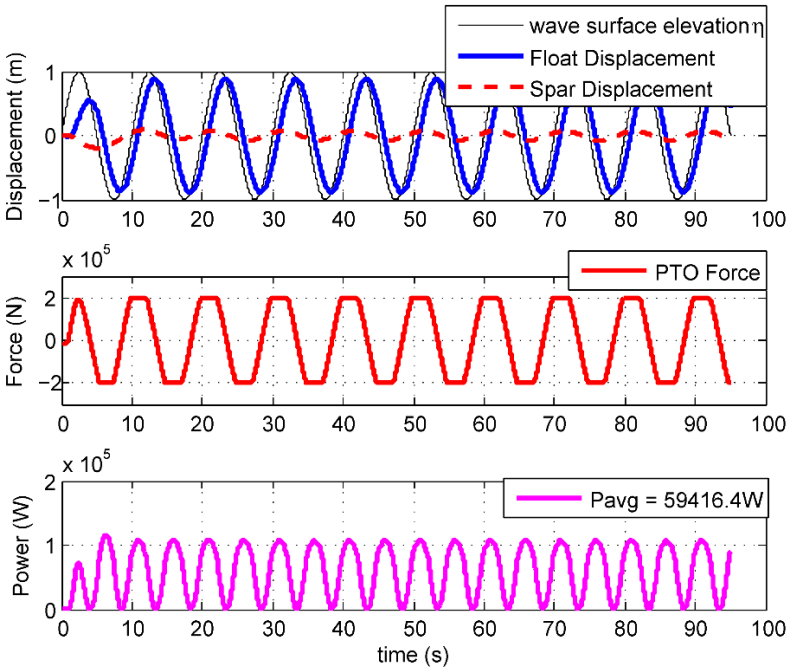

Fig. 3.6. Linear damping regular wave input. The PTO force is clipped at 200kN to represent realistic limitations of physical equipment. Because of this nonlinearity this analysis must be done in the time domain.

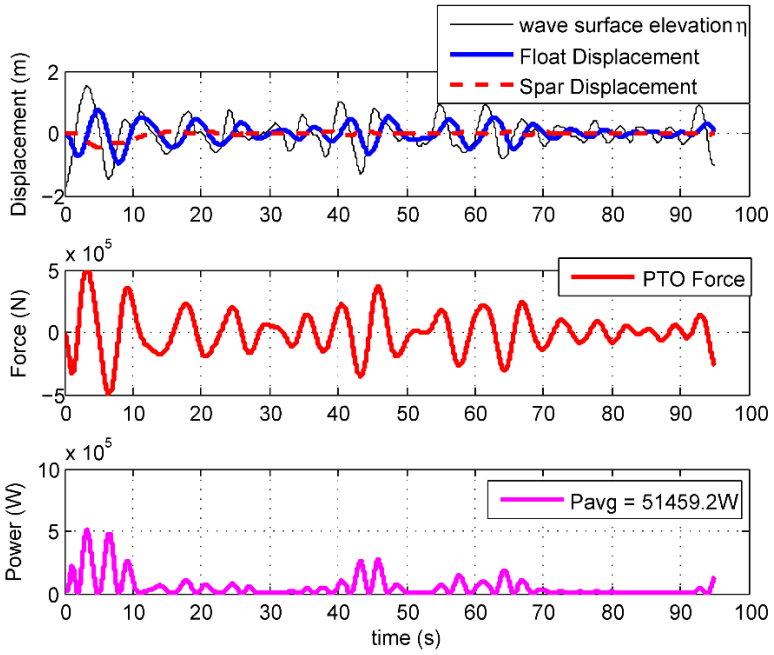

Fig. 3.7. Linear damping irregular wave input.

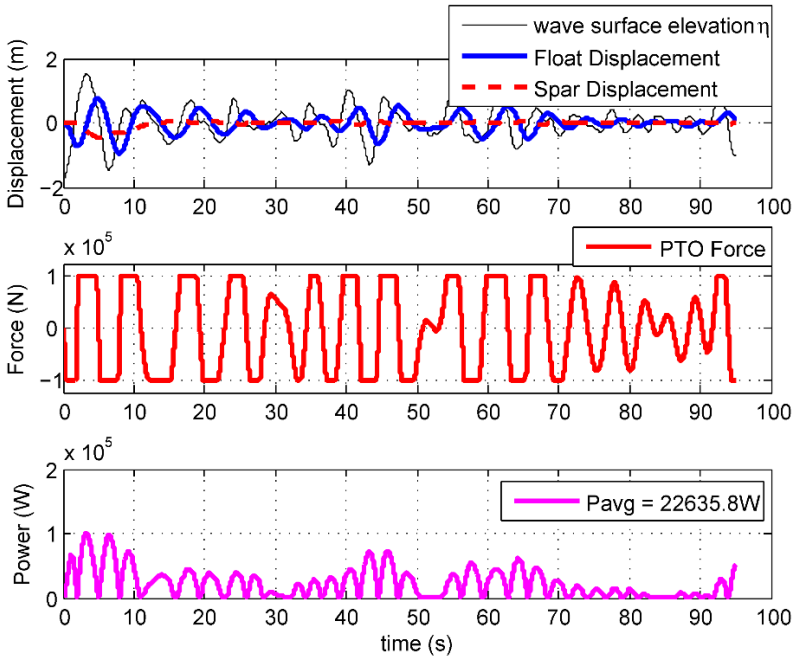

Fig. 3.8. Linear damping irregular wave input. The PTO force is clipped at 100kN to represent realistic limitations of physical equipment. Because of this nonlinearity this analysis must be done in the time domain.

3.6 Conclusions

In this research, a methodology for modeling a two body point absorber wave energy converter was outlined. The procedure included defining equations of motion and implementing them in a differential equation solver such as MATLAB/Simulink. A benefit of time domain simulation, namely the implementation of a nonlinear damping power take off model, was analyzed and results shown. This demonstrates that time-domain analysis, accommodating non-linearities in plant behavior or control, can be conducted starting from frequency domain analysis.

4 Wave Tank Testing and Model Validation

4.1 Introduction

In order to fully realize a robust, efficient, and cost effective ocean wave energy converter, considerable modeling and testing of devices will be required. Due to the size and complexity of the full scale devices, the most cost effective way to make advances is through the use of numerical modeling and scaled prototype testing. This paper takes previous numerical modeling work and attempts to validate these models with a scaled prototype tested in a large wave flume.

Wave tank testing of wave energy converters is a complicated endeavor with many challenges. There is much to be learned from previous attempts at characterizing devices and validating models. The European Marine Energy Centre (EMEC) provides a tank testing standard in [24] and the University of Edinburgh has provided tank testing guidance in [25]. The book edited by Joao Cruz [9], has a chapter dedicated to numerical and experimental modeling of WECs which is quite insightful.

The main thrust of this research is to outline the process of taking an idea of a Wave Energy Converter (WEC) and bringing it through the prototype stage of development. This includes a significant amount of numerical modeling as well as physical modeling. The outcomes of this chapter show the results of tank testing, namely the Response Amplitude Operators (RAOs) and power performance results compared with two different time domain model approaches. This model validation helps to identify the regions of operation that can be reasonably modeled, allows for the adjustment of the

model to more accurately mimic the real world, and provides confidence to change the model for future design iterations.

There is considerable interest in the development of ocean wave energy converters for remote sensing applications [26]. Currently atmospheric sensing equipment on board remote buoys is powered by a combination of solar, wind, and battery systems. Wave energy conversion technology would add to the sensing system power options. To this end, a heaving two body point absorber was chosen as a possible solution, called an Autonomous Wave Energy Converter (AWEC). A target power level was set at a nominal 200 W. Fig. 4.1 shows a block diagram of the wave flume testing inputs and outputs.

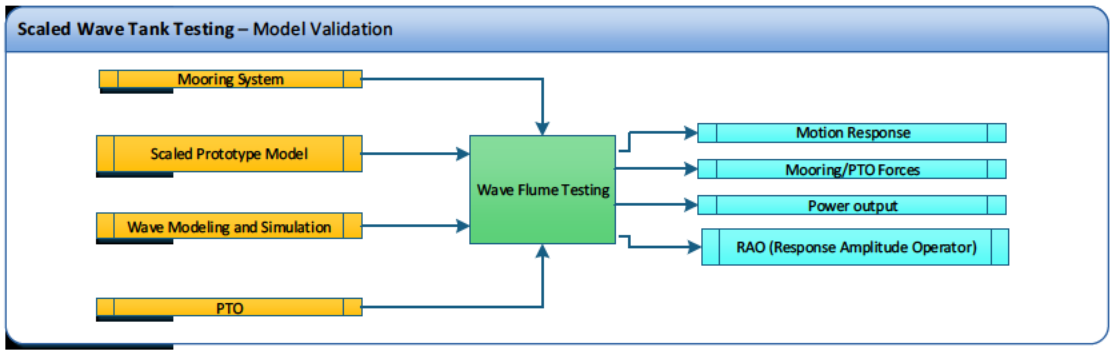

Fig. 4.1. Scaled wave tank testing block diagram. Scaled model wave tank testing for use in model validation.

4.2 Device Geometry, Scaling, Power Take Off, and Mooring

Many designs and geometry types exist for ocean wave energy extraction [5]. A heaving point absorber was chosen as the geometry to be modeled, built, and tested for this study. A point absorber is defined as a device whose horizontal extent is much smaller than one wavelength of an incoming wave. Benefits of this type of device

include a relatively simple geometry, many previous studies and built devices based on this principal, and the robust nature of such a device.

4.2.1 Geometry

Full scale geometry design of the AWEC was outlined in [27], where coastal United States locations were chosen to help inform the design. A target of 200 W continuous power was chosen to meet the general electrical load of autonomous buoys. A focus on a simple shape was pursued for reasons of cost and ease of manufacture as well as ease of modeling.

A two body approach was chosen where the relative motion between the bodies actuates the power take off. Because of limitations related to the scaled testing facility, the need for additional stability within the system, and the shallow water depth of some prospective sites, a damping plate was added. To add further stability, additional weight was added to the bottom of the device and buoyancy was added as high up as possible. This served to lower the center of gravity, while raising the center of buoyancy and thus creating a more stable device. The final full scale equivalent, and actual fabricated geometry is shown in Fig. 4.2.

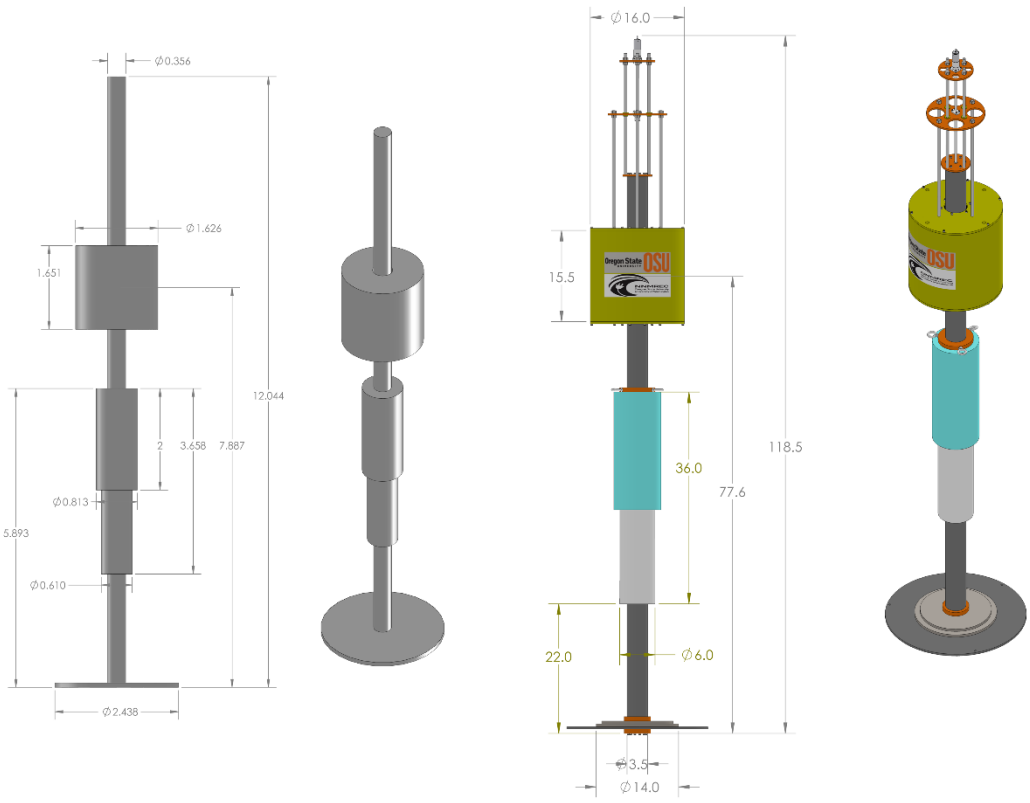

(a) (b)

Fig. 4.2. Autonomous Wave Energy Converter: (a) Full Scale and (b) ¼ scale. All dimensions in meters.

4.2.2 Scaling

To create the most realistic model of the full scale device, the largest scale factor for the prototype was chosen. This was limited by what would reasonably fit in the testing facilities. A near shore location with water depth of about 14 m -- a National Oceanic and Atmospheric Administration (NOAA) buoy location off the coast of Galveston, TX -- was used as a target location. The maximum water level in the proposed test facility divided by the water depth at the proposed site led to a scaling factor of four. That is to say that in terms of size, the target full scale device would be

four times the physical size of the prototype. In scaling the model, ideally, two non-dimensional quantities, the Froude number and the Reynolds number would be used. However, for this test, the net influence of viscous forces on body motions is considered to be negligible, and therefore the Froude scaling is assumed to be satisfied.

Having chosen the scale, the Froude Scaling method was used as introduced in [28]. As a result of this method, the prototype's physical dimensions were scaled down by a factor of four, with adjustments made to accommodate regularly available materials for ease of fabrication. Various other parameters were scaled in the process of creating a scaled model, which are shown in Table 1.

Table 1: Froude Scaling for the AWEC

Physical Parameter	Units	Factor	AWEC Factor
Length	meter (m)	λ	4
Mass	kilogram (kg)	λ^3	64
Time	second (s)	$\sqrt{\lambda}$	2
Force	Newton (N)	λ^3	64
Linear Damping	$\frac{\text{Ns}}{\text{m}}$	$\lambda^{2.5}$	32
Stiffness	$\frac{\text{N}}{\text{m}}$	λ^2	16
Power	Watts (W)	$\lambda^{3.5}$	128

Of particular note is the scaling of power. The units of power are watts, also written as

$$[W] = \frac{[kg][m]^2}{[s]^3} \tag{4.1}$$

from the scaling table we see that the power scaling then becomes

$$\frac{\lambda^3 \lambda^2}{\left(\sqrt{\lambda}\right)^3} = \lambda^{3.5} \tag{4.2}$$

so, from the target of 200 W continuous power and a scale factor of four the scaled output power is 1.5625 W. Because of this large power scaling factor, extra care is required to implement the scaled power take off system.

4.2.3 Power Take Off

The Power Take Off (PTO) system is responsible for converting the force created by the motion of a WEC to some useful power. As is the case for a heaving point absorber, this often requires the translation of linear motion to rotary motion. There are many ways that this can occur including direct drive solutions as well as intermediate energy translation solutions such as hydraulic systems. A study of direct drive solutions is performed in [29]. A linear generator system is detailed in [30] and [31]. For the project documented in this chapter, a ball screw spindle drive was chosen coupled to a high efficiency brushed DC motor. At the scale of the built device this provided the highest efficiency, lowest cost, and easiest implementation of readily available products. For example, one beneficial aspect of this PTO device was the readily available drive

electronics consisting of a four quadrant servo-controller. This provided an easily adaptable platform for the implementation of various control schemes.

4.2.4 Mooring

The mooring of wave energy conversion devices is very important and should not be taken lightly. Mooring can significantly affect the power production, survivability, environmental impact, and cost. An overview of a design approach is given in [32]. Mooring details for the scaled device is shown in section 4.4.3.

4.3 Linear Test Bed Testing

Due to the complex nature of a wave energy converter, there is a lot of useful information that can be gleaned from testing before the device ever enters the water. For this particular project the benefits of dry testing served two purposes. First, it allowed for the testing of most system components in a situation similar to those it sees in the water. Second, it allowed for the characterization of system losses, which are a significant contributing factor affecting the performance of a device. These losses can take many forms, but mostly can be attributed to friction, gearbox, and generator inefficiencies. In an attempt to characterize the system losses, as well as do a complete system validation, a Linear Test Bed (LTB) located in the Wallace Energy Systems and Renewables Facility was used as shown in Fig. 4.3. An overview of the Linear Test Bed is given in [33].

Fig. 4.3. Testing in the Linear Test Bed (LTB)

4.3.1 Power Delivered to the Load

A useful measure of device performance is the electrical power delivered to the load for different operating conditions. A sweep of constant velocities and different load conditions were conducted as trials. Power was measured as the product of the voltage across and current through the DC motor load resistance. This was then scaled using Froude scaling to obtain the full scale equivalent power. Fig. 4.4 shows the results from this test. Note that the power generally increases as the velocity increases as expected. Also notice that the load resistance near the internal resistance of the generator (7.41 ohms) provides the max power from the generator.

	0.52 m/s	0.58 m/s	0.67 m/s
3.5 ohm	222	344	619
7 ohm	269	415	748
10.5 ohm	267	415	749
14 ohm	251	394	706
28 ohm	188	294	529
56 ohm	118	186	332

Full Scale Equivalent Power (W)

Fig. 4.4. Power Delivered to the Load in Watts. Power generally increases as velocity increases. A load resistance near the generator internal resistance (7.41 ohms) provides max power.

4.3.2 Efficiency Test

In order to estimate the total efficiency for the system, a series of tests were conducted. A profile was loaded into the LTB to cause a constant velocity between the float and the spar. For each trial, a velocity and a load condition were chosen, and the efficiency was calculated as follows

$$P_{in} = P_k + P_r + P_{loss} + P_{elec} \tag{4.3}$$

$$P_{elec} = V_{gen} I_{gen} \tag{4.4}$$

where P_{in} is the power input to the system by the LTB, P_k is the rate of change of the linear kinetic energy present in the system which is zero for a constant velocity, P_r is the rate of change of the rotational kinetic energy in the system which is zero for a constant velocity, P_{loss} is the power losses in the system, and P_{elec} is the power measured out of the generator.

$$P_{loss} = P_{in} - P_{elec} \tag{4.5}$$

$$\eta = \frac{P_{elec}}{P_{elec} - P_{loss}} \tag{4.6}$$

where η is the overall system efficiency.

Fig. 4.5 shows the results of these trials. Generally, as the speed increased, so did the efficiency. Also, the efficiency peaks for the generator load at approximately double the generator internal resistance (7.41 ohms).

	0.52 m/s	0.58 m/s	0.67 m/s
3.5 ohm	15	16	22
7 ohm	21	23	32
10.5 ohm	23	25	41
14 ohm	26	27	39
28 ohm	22	22	47
56 ohm	13	14	29

Efficiency %

Fig. 4.5. Total PTO efficiency in % for different velocities and loads. As speed increases, so does efficiency. The efficiency peaks for the generator load at approximately twice the generator internal resistance (7.41 ohms).

4.3.3 Estimated Damping Values Due to Losses

In order to include the losses in any model of the overall system, an estimate of those losses should be included. Although these losses are nonlinear, a linear damping term is the easiest way to implement the estimated losses and is a good first pass approximation. This term can be estimated as follows

$$F_{loss} = B_{loss} v \tag{4.7}$$

$$P_{loss} = F_{loss} v = B_{loss} v^2 \tag{4.8}$$

$$B_{loss} = \frac{P_{loss}}{v^2} \tag{4.9}$$

where F_{loss} is the equivalent loss force in the system; B_{loss} is the loss damping and captures friction and other high order loss mechanisms; v is the linear velocity; and P_{loss} is the power lost due to the inefficiencies of the system. Again, the velocity and load conditions were swept with the resulting estimates for B_{loss} shown in Fig. 4.6. As expected, the higher speeds produced a lower estimated damping value. A mean value of 2000 $\frac{Ns}{m}$ was used in both AQWA and MATLAB/Simulink full scale models.

	0.52 m/s	0.58 m/s	0.67 m/s
3.5 ohm	2648	2262	941
7 ohm	2457	2219	889
10.5 ohm	2432	2032	770
14 ohm	2318	2039	824
28 ohm	2391	2275	757
56 ohm	2274	2068	819

Damping (Ns/m)

Fig. 4.6. Estimated Loss Damping Values for a Sweep of Velocity and Load Values. Higher speeds produced lower estimated damping values.

4.4 Wave Tank Testing Facilities

The next step in the model validation process was testing the scaled AWEC model in the large wave flume located in the O.H. Hinsdale Wave Research Laboratory (HWRL) at Oregon State University (OSU). The HWRL has performed similar wave energy converter testing in the large wave flume as detailed in [12], which made for a relatively smooth process for testing. Data from the test trials were recorded for the three major data acquisition systems included in the testing. This included the wave flume, optical tracking, and device performance data which will be reviewed in the following sections.

4.4.1 Large Wave Flume

The large wave flume is one of the largest of its kind in North America and measures 104 m long by 3.7 m wide and 4.6 m deep. The wave maker is hydraulic-piston actuated, and capable of creating regular, irregular, tsunami, and user defined wave types. The period range is from 0.5 to 10 seconds with a maximum wave height of 1.6 m at a 7 second period. A 1:12 concrete beach was selected to minimize reflections within the

tank. A water depth of 3.353 m was chosen as this was the maximum reasonable depth for testing in the flume.

For the AWEC testing setup, several data acquisition measurements related to the wave tank were included. A wave maker start signal, wave maker displacement, a wave gauge located at the wave maker, and a pressure sensor level signal were all recorded. Additionally, three resistance type self-calibrating wave gauges located near the tank wall near the device under test were recorded. All signals were logged with a data acquisition system with a sampling rate of 50 Hz. In the logging of data the goal is typically to get the most accurate measure of the quantity desired with the smallest amount of noise recorded. Because most of the frequencies of interest in the AWEC model are much lower than most electrical noise, a low-pass filter is generally effective in eliminating most of the noise from the acquired signal. Fig. 4.7 shows the basic geometry and layout of the large wave flume, with the location of the wave gauges, device under test (model AWEC), and optical tracking system (PhaseSpace).

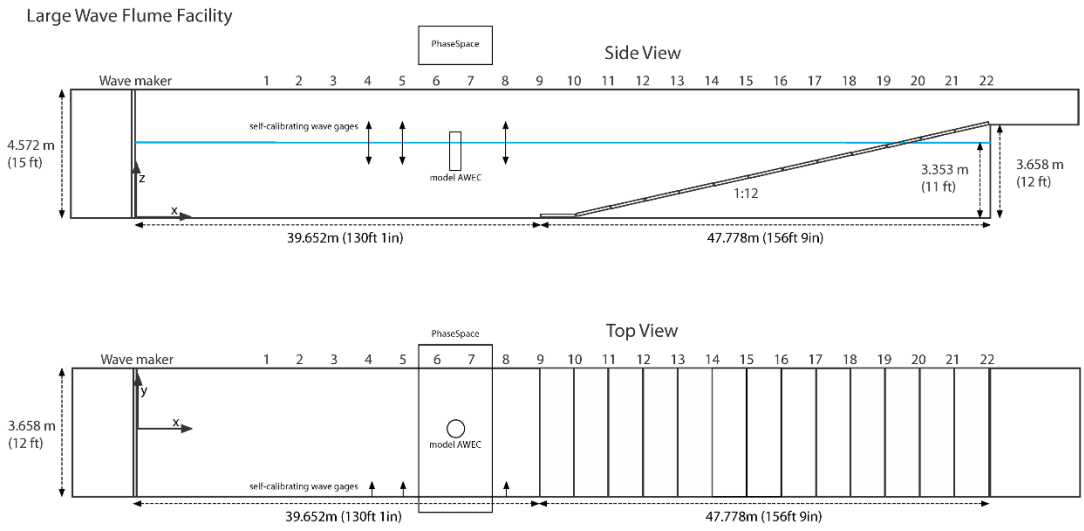

Fig. 4.7. Large Wave Flume Configuration

4.4.2 Optical Motion Capture System

In attempting to validate numerical models of the AWEC system, it was very important to have confidence in the motion tracking data of the bodies under test. A PhaseSpace optical motion capture system was used for this purpose. This system, designed for the entertainment industry, allows high resolution tracking of rigid bodies. Twenty-seven uniquely identified active LED markers viewed by eight cameras surrounding the device describe the PhaseSpace setup. Motion data is recorded at a 480 Hz sampling rate. Previous tests found a 6-sigma accuracy of 0.9 mm for all targets within a 1.2 m radius, and 1.3 mm accuracy up to a 2.5 m radius [34]. Each body of the AWEC was uniquely identified for six degrees of freedom in relation to the reference coordinate definition square. Fig. 4.8 shows the PhaseSpace setup on the left and a computer image showing the cameras and markers for each LED on the right.

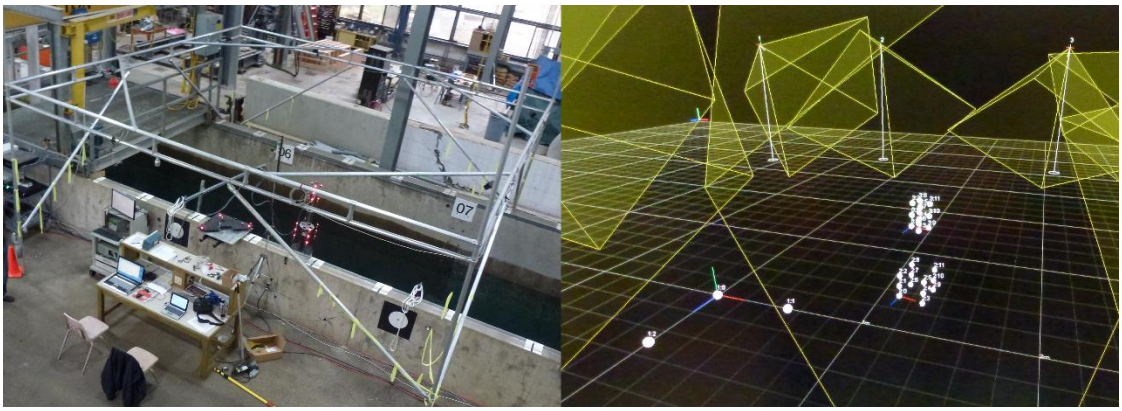

(a) (b)

Fig. 4.8. Optical Motion Tracking: (a) Setup in HWRL and (b) screen capture of tracking markers.

4.4.3 Mooring

For testing in the large wave flume at the O.H. Hinsdale Wave Research Laboratory, a three point mooring system was constructed and implemented. Each line was installed in pretension in a horizontal plane with a 120 degree angle between the lines. The aft mooring line was parallel to the wave tank walls. Each line had a pulley system which led to a load cell on the edge of the tank. Mooring force was recorded for each line. Each line consisted of a 1.5 m un-stretched length of surgical tubing and a length of stiff rope. Experimental testing on the surgical tubing revealed an estimated stiffness of 520 N/m for a full scale equivalent, obtained using Froude scaling. Each line was set in a pretension of 0.5 m. That is to say each surgical tubing section equilibrium length under test was 2 m.

4.4.4 Device Performance Data

Device performance data from the AWEC was also recorded with the data acquisition system. In all, sixteen channels of data were recorded at a 50 Hz sampling rate using

the HWRL data acquisition system. The signals can be broken into two categories, namely signals related to the power take off and signals related to the mooring.

Several signals related to the power take off, consisting of a lead screw, gearbox, generator, and encoder were logged. From the encoder data, position, velocity, and acceleration signals were recorded, which describe the relative motion between the two bodies: the float and spar. Voltages and currents were logged including the system bus voltage, power supply current, and load current. The general setup for the PTO circuit is show in Fig. 4.9. Several signals related to the 4-quadrant drive were logged including the drive current, drive velocity, commanded current, and the enable command. Additionally each of the three mooring lines had a load cell attached, and this mooring force was also recorded.

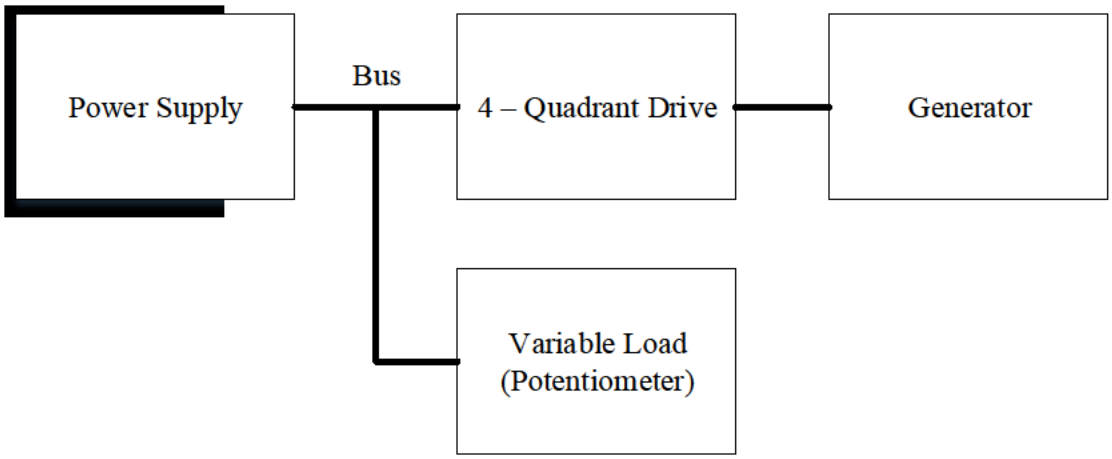

Fig. 4.9. Power Take Off circuit.

4.5 Wave Tank Testing Procedure

Wave tank testing occurred over a two week period in the O.H. Hinsdale Wave Research Laboratory. Three and a half days were dedicated to the setup of the wave tank. This included installation of the mooring system, installation of the device under test, installation of the optical motion tracking system, installation of the wave gauges and related wave tank systems, filling of the tank, and calibration of the system. Six days were then dedicated to experimental testing which is outlined below. Fig. 4.10 shows the device under test.

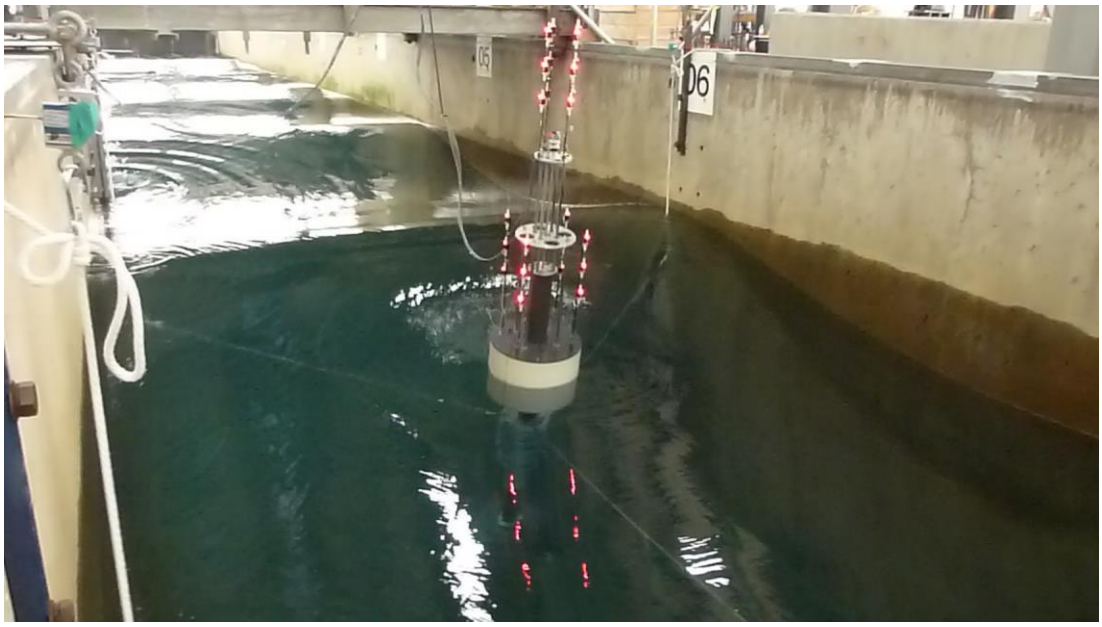

Fig. 4.10. AWEC testing in the Hinsdale Wave Research Laboratory at Oregon State University.

4.5.1 Experimental Methodology and Procedure

Each individual running of waves was considered to be a trial. Each trial was a member of an experiment. In all, there were nine experiments conducted with a total of

one hundred and forty-three trials. All trials were run with either monochromatic or Pierson-Moskowitz spectral wave input. In general, with a few exceptions, the length of run was set to 200 waves (based on the dominant period if spectral). In addition to the 200 waves, there was a ramp up time and ramp down time associated with the data acquisition and the wave maker. Also in general, if control was to be implemented in the run, which was the case for most trials, the first ten percent of the trial was run with the control off. At ten percent of the total trial length the control was then activated and applied for the duration of the trial.

4.5.2 Types of Trials Conducted

Of the hundred and forty three trials conducted throughout the testing, the bulk of the trials fit into four experiments. In an attempt to characterize the device, a sweep of wave height and period was conducted with a monochromatic input creating a five by five matrix. Also in characterizing the device, a sweep of irregular waves was performed, sweeping significant wave height and dominant wave period for a similar five by five matrix of values. The final experiments were conducted as an exercise in testing a binary and ternary control scheme for generating more power from the AWEC. The results of these last two experiments will be published separately.

4.6 Wave Tank Testing Results

The main thrust of this work involved the model validation of a scaled prototype using numerical modeling techniques. Two numerical modeling tools, ANSYS AQWA and MATLAB/Simulink, were used to run full scale equivalent models of the AWEC.

Results from the tank testing were scaled up for comparison with the numerical results using Froude scaling. Because of the discrepancies between the commanded and measured wave heights and periods, input to the numerical models were made to match full scale equivalent measured wave tank wave heights and periods.

4.6.1 Commanded vs. Measured Wave Tank Results

For regular wave inputs wave gauge readings were taken on the wave maker side of the AWEC. A desired period and wave height was given to the wave maker operator for each trial. The resulting wave surface elevation was recorded at the location of the wave gauge closest to the AWEC. All wave gauge data was filtered using a band-pass Butterworth filter. The resulting measurement of the wave period closely matched the expected period, however, the measured wave height deviated from the expected by as much as 29%. Furthermore, for different periods given the same expected wave height, the measured average wave height varied. Because of these results, all time domain simulations done in both AQWA and MATLAB/Simulink received the scaled measured input wave height in order to compare the theoretical results to measured results.

For irregular wave input, a similar process was followed. Because of restrictions on the operation of the wave maker, two of the trials in the matrix were unable to be completed. Results showed that there is significant error in both peak period and significant wave height with a max error of 27% and 35% respectively. In order to compare the hardware results with the numerical modeling, a scaled time series of measured wave heights was used as the input to the AQWA and MATLAB/Simulink numerical modeler.

4.6.2 Max Damping Value

For purposes of model validation and characterization of the system a fixed damping value was needed in order to conduct the tests. In order to achieve a fixed damping value the 4-quadrant drive was set in a current control (i.e., torque control) operating mode. A velocity proportional damping term $B\ \left(\frac{Ns}{m}\right)$ was then used to set the desired torque command to the motor. Early tests were run using a monochromatic wave input to the system. As the trial progressed, after approximately every ten waves the damping values were stepped up. Fig. 4.11 shows the results from a damping sweep for two different monochromatic input waves, one with a full scale wave height of 1 m and period of 4 s, and one with a full scale wave height of 2 m and period of 6 s. As the plot shows the maximum full scale damping value for either case was near $B = 1600\,\frac{Ns}{m}$, which was then chosen as the base damping value to be used for all sweeps of wave height and period, both monochromatic and spectral.

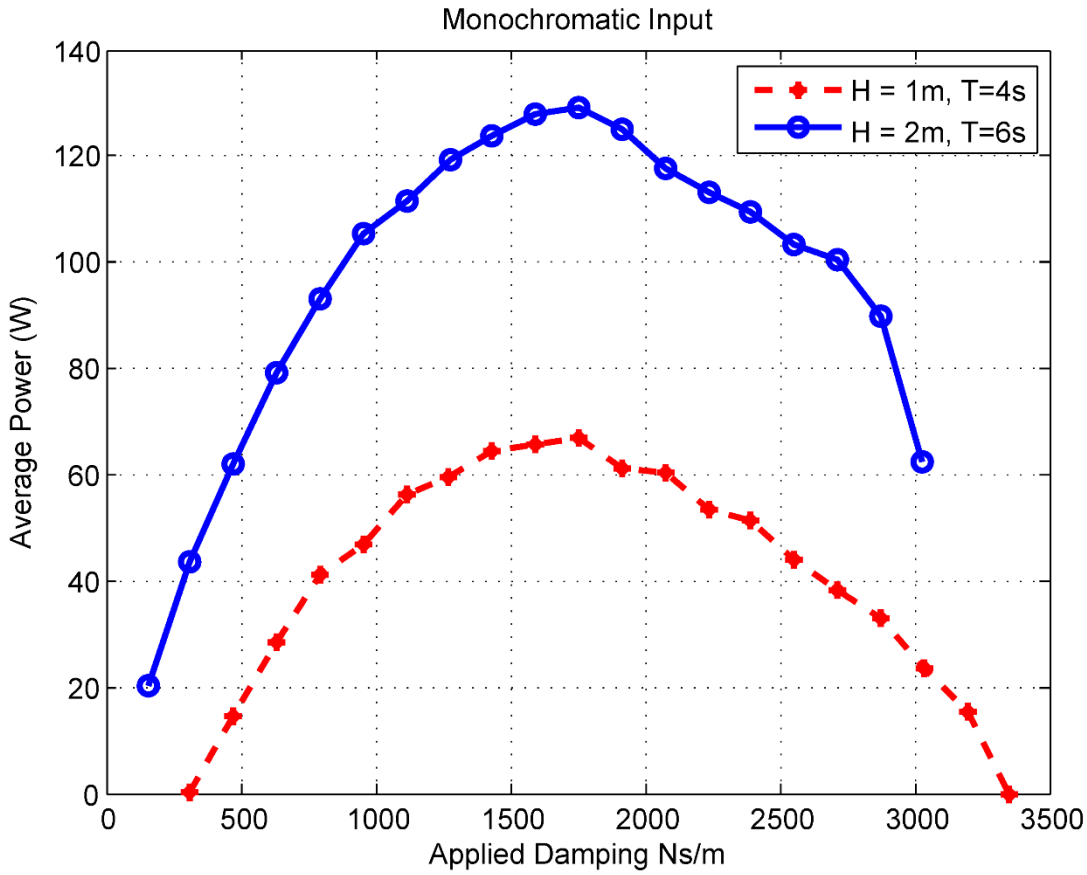

Fig. 4.11. Average Power vs. Damping for two monochromatic wave inputs.

4.6.3 Response Amplitude Operators (RAOs)

Testing in regular waves gives insight into the behavior of the system in a relatively controlled environment, controlled by two parameters namely wave height and wave period. One measure of the performance of such regular wave tests is the calculation of the Response Amplitude Operator (RAO). The RAO is essentially a transfer function describing the relationship between an input and output characteristic of the components of the device of interest. Traditionally, in ship design, RAOs are often used in the design stage to determine modifications that may need to occur for

safety reasons. In ocean wave energy conversion RAOs can be useful in design for maximum power extraction. For this study, because of the nature of the point absorber, the heave motion was identified as the pertinent motion for energy capture and thus the RAO was calculated for each body, namely the float heave and spar heave as follows

$$RAO = \frac{\zeta}{\eta} \quad \left[\frac{m}{m}\right] \tag{4.10}$$

where ζ is the body heave amplitude and η is the incoming wave amplitude. For each body the time series response was analyzed to find the positive zero crossings. Then for each period the amplitude of the waveform was calculated. The average of these values was then determined to be the body average heave amplitude. A similar process was used to obtain the average incoming wave amplitude.

As part of the model validation process, three sets of RAOs were calculated and compared for each rigid body. First, the tank test results of wave surface elevation as measured by the resistance wave gauges was used with the optical motion tracking information from PhaseSpace for the heave amplitude of each body. Second, time domain simulations from ANSYS AQWA-NAUT were used to calculate the RAO. Third, a MATLAB/Simulink time domain simulator based on the ANSYS AQWA LINE hydrodynamic frequency domain parameters was conducted. The methodology and a review of this modeling process is outlined in [21]. The RAOs for the three data sets are shown in Fig. 4.12.

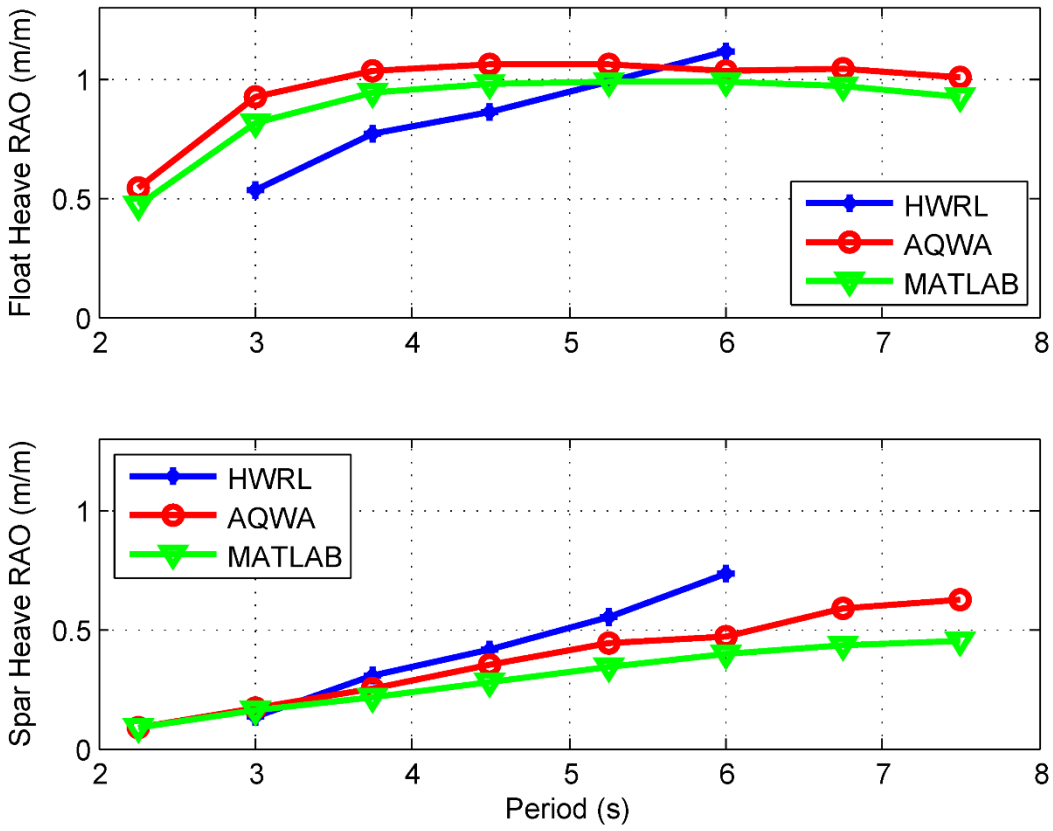

Fig. 4.12. RAOs for HWRL, AQWA, and MATLAB.

4.6.4 Power Characteristics

One key measure of the performance of a wave energy converter is its average power output. This is particularly important for an autonomous application because a sensor package may rely on a certain baseline average power production for consumption. In characterizing a device it is most useful to look at the power output for irregular waves because this will be the case for any real world conditions. As outlined earlier, a sweep of significant wave height and dominant period was done to create a 5x5 matrix of system outputs. Power production was calculated by measuring

the bus voltage and the currents in the circuit and then calculating the power generated by the PTO. The result is the total power produced including all losses. Time domain simulations were then performed using ANSYS AQWA-NAUT and a time domain simulation tool in MATLAB/Simulink developed by the author described in [35] in an attempt to simulate the testing environment. As described earlier, the losses implemented in the numerical models were estimated as additional damping in the system. The result is a power matrix plot showing the average power output for different combinations of significant wave height and dominant period irregular wave inputs for one hardware test and two hydrodynamic modeling exercises as shown in Fig. 4.13.

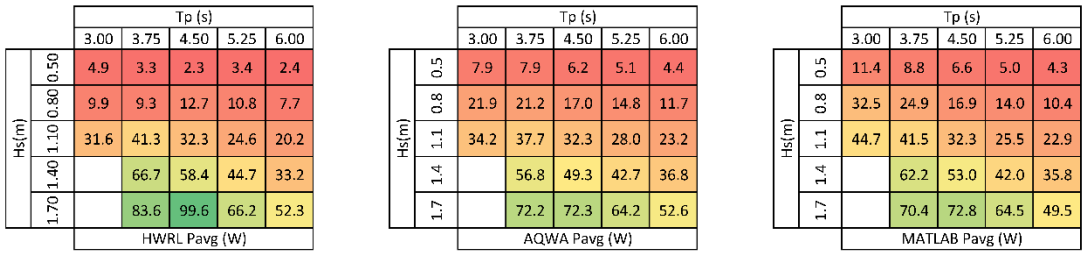

(a) (b) (c)

Fig. 4.13. Power Matrix for Irregular wave input: (a) HWRL wave tank testing, (b) AQWA model, and (c) MATLAB model.

In order to quantify the differences between the model and the measured data, the percent error was calculated between the different methods. Fig. 4.14 shows the % error between the measured data and AQWA simulated data. As shown, the match is quite good at the nominal case. As lower significant wave heights and peak periods are analyzed the error generally gets larger, with the AQWA model over-predicting the power output of the system. As significant wave heights increase and peak periods

decrease the trend shows an AQWA under-prediction of power output.

		Tp (s)				
		3.00	3.75	4.50	5.25	6.00
Hs(m)	0.50	60.8	138.9	167.3	49.3	85.2
	0.80	122.1	128.1	34.0	37.2	52.5
	1.10	8.3	-8.8	0.0	13.9	14.6
	1.40		-14.8	-15.5	-4.5	10.6
	1.70		-13.6	-27.4	-2.9	0.6
		% error between HWRL and AQWA				

Fig. 4.14. Percent error between measured tank testing data and AQWA model data. AQWA over-predicts for lower significant wave heights and dominant periods. AQWA under-predicts for higher significant wave heights and dominant periods.

4.7 Conclusions

This work provides an overview of linear test bed and wave tank testing procedures, as well as model validations stemming from the tank testing results. Design and testing methodologies were overviewed and results for characterizing a WEC and validating a model were given. Results include power output results from irregular wave input, and response amplitude operator (RAO) results from regular wave input. Numerical methods were shown to have relatively accurate results around a nominal operating point with increased error in the model as the conditions varied from the nominal. Tank testing of the AWEC showed electrical power generation performance below the targeted level although there was good agreement with simulated results.

Future work includes refinements to the hydrodynamic design and the PTO system to improve power generation.

5 Conclusion

A design and testing methodology for the development of ocean wave energy converters has been developed and implemented. Initial modeling was conducted on a full scale utility sized WEC. Wave tank testing was conducted on a one quarter scale autonomous device and model validation was performed.

The first step in the process was the frequency domain analysis, where a general sense of the system performance was gathered. ANSYS AQWA was used to obtain the results. Results of RAOs and power as a function of frequency were presented as well as the hydrodynamic properties of the device. This would allow for relatively fast shape optimization.

Next, a time domain model was developed using MALTAB/Simulink. This model is based on the results from the frequency domain. Non-linearities were introduced into the model of the power take off, which were not possible in the frequency domain. This provided a more realistic look at the system outputs.

Finally, a scaled prototype of an Autonomous Wave Energy Converter (AWEC) was designed, built, and tested. Both frequency domain and time domain numerical simulations were used to model the AWEC. Testing of the physical prototype was conducted both in the Wallace Energy Systems and Renewables Facility (WESRF) and the O.H. Hinsdale Wave Research Laboratory (HWRL), both located at Oregon State University. Results showed reasonable agreement between the time domain modeling and wave tank testing results near a nominal operating point.

5.1 Recommendation for Future Work

There are many directions that future work could go from this project. A very rich data set was gathered during the hardware testing and much more analysis could be performed on this data. One example is the mooring load cell data, which could be used to modify and enhance the numerical mooring model. Other further improvements to the numerical model could be implemented to strengthen the match with hardware. A more complex model of losses in the system including the power take off system could be beneficial. Introduction of nonlinear elements in the mooring time domain model would also be an improvement. The physical prototype could then be put back onto the linear test bed and conditions could be run to match the wave tank testing to further validate the numerical model.

Another opportunity for future work could be additional tests run with the same or modified hardware. The physical hardware from the test is in good condition and would be ready for future testing. Small improvements, for example in the mechanical bushings, could result in higher efficiencies for future tests. These bushings could be replaced with some sort of bearing to help reduce losses. Also, the surface between the spar and float could be investigated for a more appropriate system to reduce losses. More complex control algorithms could also be explored using the existing hardware. Improvements in the hydrodynamic design and PTO design could also significantly improve power generation.

6 Bibliography

[1] "IEA - Publication:- Key World Energy Statistics 2012." [Online]. Available: http://iea.org/publications/freepublications/publication/name,31287,en.html. [Accessed: 21-Jun-2013].

[2] A. Clément, P. McCullen, A. Falcão, A. Fiorentino, F. Gardner, K. Hammarlund, G. Lemonis, T. Lewis, K. Nielsen, S. Petroncini, M.-T. Pontes, P. Schild, B.-O. Sjöström, H. C. Sørensen, and T. Thorpe, "Wave energy in Europe: current status and perspectives," *Renewable and Sustainable Energy Reviews*, vol. 6, no. 5, pp. 405–431, Oct. 2002.

[3] S. H. Salter, "Wave power," *Nature*, vol. 249, no. 5459, pp. 720–724, Jun. 1974.

[4] Paul T. Jacobson, George Hagerman, and George Scott, "Mapping and Assessment of the United States Ocean Wave Energy Resource," DOE/GO/18173-1, 1060943, Dec. 2011.

[5] A. F. de O. Falcão, "Wave energy utilization: A review of the technologies," *Renewable and Sustainable Energy Reviews*, vol. 14, no. 3, pp. 899–918, Apr. 2010.

[6] "Commercialization Program | Oregon Wave Energy Trust." [Online]. Available: http://www.oregonwave.org/commercialization-program/. [Accessed: 22-Jun-2013].

[7] J. Falnes, *Ocean waves and oscillating systems : linear interactions including wave-energy extraction*. Cambridge: Cambridge University Press, 2005.

[8] M. McCormick, *Ocean engineering mechanics : with applications*. Cambridge ;;New York: Cambridge University Press, 2010.

[9] J. Cruz, *Ocean Wave Energy: Current Status and Future Prespectives*, 1st ed. Springer, 2008.

[10] K. Ruehl, T. K. A. Brekken, B. Bosma, and R. Paasch, "Large-scale ocean wave energy plant modeling," in *Innovative Technologies for an Efficient and Reliable Electricity Supply (CITRES), 2010 IEEE Conference on*, 2010, pp. 379–386.

[11] Eidsmoen, "Simulation of a slack-moored heaving-buoy wave-energy converter with phase control," Division of Physics, Norwegian University of Science and Technology, 1996.

[12] K. Rhinefrank, A. Schacher, J. Prudell, E. Hammagren, Z. Zhang, C. Stillinger, T. Brekken, A. von Jouanne, and S. Yim, "Development of a Novel 1:7 Scale

Wave Energy Converter," *ASME Conf. Proc.*, vol. 2011, no. 44373, pp. 935–944, Jan. 2011.

[13] A. Babarit, J. Hals, M. J. Muliawan, A. Kurniawan, T. Moan, and J. Krokstad, "Numerical benchmarking study of a selection of wave energy converters," *Renewable Energy*, vol. 41, pp. 44–63, May 2012.

[14] "ANSYS Aqwa." [Online]. Available: http://www.ansys.com/Products/Other+Products/ANSYS+Aqwa. [Accessed: 01-Jun-2012].

[15] "3D CAD Design Software SolidWorks." [Online]. Available: http://www.solidworks.com/. [Accessed: 13-Jun-2012].

[16] N. O. and A. A. US Department of Commerce, "National Data Buoy Center." [Online]. Available: http://www.ndbc.noaa.gov/. [Accessed: 25-Jun-2012].

[17] "Wamit, Inc. - The State of the Art in Wave Interaction Analysis." [Online]. Available: http://www.wamit.com/. [Accessed: 01-Jun-2012].

[18] C. C. Mei, "Numerical Methods in Water-Wave Diffraction and Radiation," *Annual Review of Fluid Mechanics*, vol. 10, no. 1, pp. 393–416, 1978.

[19] J. Fitzgerald and L. Bergdahl, "Including moorings in the assessment of a generic offshore wave energy converter: A frequency domain approach," *Marine Structures*, vol. 21, no. 1, pp. 23–46, Jan. 2008.

[20] V. Gomez, R. Guanche, C. Vidal, and I. Eguinoa, "Numerical simulation of a submerged wave energy converter under irregular wave conditions," in *OCEANS, 2011 IEEE - Spain*, 2011, pp. 1 –10.

[21] B. Bosma, Z. Zhang, T. K. A. Brekken, H. T. Ozkan-Haller, C. McNatt, and S. C. Yim, "Wave energy converter modeling in the frequency domain: A design guide," in *2012 IEEE Energy Conversion Congress and Exposition (ECCE)*, 2012, pp. 2099 –2106.

[22] W. Cummins, "The impulse response function and ship motions," *Schiffstechnik*, vol. 9, pp. 101–109, 1962.

[23] J. Falnes, *Ocean waves and oscillating systems: linear interactions including wave-energy extraction*. Cambridge University Press, 2002.

[24] "Tank Testing of Wave Energy Conversion Systems : EMEC: European Marine Energy Centre." [Online]. Available: http://www.emec.org.uk/tank-testing-of-wave-energy-conversion-systems/. [Accessed: 03-Dec-2012].

[25] G. Payne and D. Ingram, “Best practice guidelines for tank testing of wave energy converters,” *The Journal of Ocean Technology*, vol. 4/4, pp. 38–70, 2009.

[26] P. Hart, “ONT – June 2012 : Autonomous Powerbuoys: Wave Energy Converters As Power Sources For The Next Generation Of Ocean Observatories.” [Online]. Available: http://virtual.ocean-news.com/article/Autonomous_Powerbuoys%3A_Wave_Energy_Converters_As_Power_Sources_For_The_Next_Generation_Of_Ocean_Observatories/1081385/114319/article.html. [Accessed: 09-May-2013].

[27] T. M. Lewis, A. von Jouanne, and T. K. A. Brekken, “Modeling and control of a slack-moored two-body wave energy converter with finite element analysis,” in *2012 IEEE Energy Conversion Congress and Exposition (ECCE)*, 2012, pp. 938–945.

[28] J. Newman, *Marine hydrodynamics*. MIT Press, 1977.

[29] K. Rhinefrank, A. Schacher, J. Prudell, T. K. A. Brekken, C. Stillinger, J. Z. Yen, S. G. Ernst, A. von Jouanne, E. Amon, R. Paasch, A. Brown, and A. Yokochi, “Comparison of Direct-Drive Power Takeoff Systems for Ocean Wave Energy Applications,” *IEEE Journal of Oceanic Engineering*, vol. 37, no. 1, pp. 35 –44, Jan. 2012.

[30] C. Bostrom, R. Waters, E. Lejerskog, O. Svensson, M. Stalberg, E. Stromstedt, and M. Leijon, “Study of a Wave Energy Converter Connected to a Nonlinear Load,” *IEEE Journal of Oceanic Engineering*, vol. 34, no. 2, pp. 123–127, 2009.

[31] C. Bostrom, B. Ekergard, R. Waters, M. Eriksson, and M. Leijon, “Linear Generator Connected to a Resonance-Rectifier Circuit,” *IEEE Journal of Oceanic Engineering*, vol. 38, no. 2, pp. 255–262, 2013.

[32] L. Johanning, G. H. Smith, and J. Wolfram, “Mooring design approach for wave energy converters,” *Proceedings of the Institution of Mechanical Engineers, Part M: Journal of Engineering for the Maritime Environment*, vol. 220, no. 4, pp. 159–174, Dec. 2006.

[33] P. M. (Peter M. Hogan, “A linear test bed for characterizing the performance of ocean wave energy converters,” Thesis, 2007.

[34] K. Rhinefrank, A. Schacher, J. Prudell, E. Hammagren, C. Stillinger, D. Naviaux, T. Brekken, and A. von Jouanne, “Scaled wave energy device performance evaluation through high resolution wave tank testing,” in *OCEANS 2010*, 2010, pp. 1–6.

[35] B. Bosma, T. Brekken, H. T. Ozkan-Haller, and S. C. Yim, "Wave Energy Converter Modeling in the Time Domain: A Design Guide," in *IEEE Conference on Technologies for Sustainability*, Portland, OR, 2013.